JCB Journal of Cell Biology

ARTICLE

SGEF forms a complex with Scribble and Dlg1 and regulates epithelial junctions and contractility

Sahezeel Awadia[1], Farah Huq[2], Torey R. Arnold[2], Silvia M. Goicoechea[1], Young Joo Sun[3], Titus Hou[3], Gabriel Kreider-Letterman[1], Paola Massimi[4], Lawrence Banks[4], Ernesto J. Fuentes[3], Ann L. Miller[2], and Rafael Garcia-Mata[1]

The canonical Scribble polarity complex is implicated in regulation of epithelial junctions and apical polarity. Here, we show that SGEF, a RhoG-specific GEF, forms a ternary complex with Scribble and Dlg1, two members of the Scribble complex. SGEF targets to apical junctions in a Scribble-dependent fashion and functions in the regulation of actomyosin-based contractility and barrier function at tight junctions as well as E-cadherin–mediated formation of adherens junctions. Surprisingly, SGEF does not control the establishment of polarity. However, in 3D cysts, SGEF regulates the formation of a single open lumen. Interestingly, SGEF's nucleotide exchange activity regulates the formation and maintenance of adherens junctions, and in cysts the number of lumens formed, whereas SGEF's scaffolding activity is critical for regulation of actomyosin contractility and lumen opening. We propose that SGEF plays a key role in coordinating junctional assembly and actomyosin contractility by bringing together Scribble and Dlg1 and targeting RhoG activation to cell–cell junctions.

Introduction

Epithelial cells form tightly packed sheets of uniformly polarized cells, with an apical membrane contacting the environment, lateral membranes held together by specialized cell–cell junctions, and basal membranes anchored to other cells or the extracellular matrix (Rodriguez-Boulan and Macara, 2014). The establishment of apicobasal polarity in epithelial cells is regulated by three highly conserved protein complexes: PAR, Crumbs, and Scribble (Bilder et al., 2003). These polarity complexes contain proteins that act as scaffolds to recruit other binding partners, including the Rho GTPases, to build spatially distinct signaling complexes. Rho GTPases act as molecular switches that cycle between an inactive GDP-bound and an active GTP-bound form. Activation of Rho proteins is mediated by Rho guanine nucleotide exchange factors (GEFs), whereas the Rho GTPase activating proteins (GAPs) mediate their inactivation (Rossman et al., 2005; Tcherkezian and Lamarche-Vane, 2007). Rho GTPases have been implicated in most steps of the establishment and maintenance of cell polarity, as well as in junction formation. Importantly, there is an extensive interdependence between the Rho GTPases and members of the polarity complexes during cell polarization (Iden and Collard, 2008; Mack and Georgiou, 2014). However, the mechanisms regulating this interdependence are poorly understood.

The Scribble complex is highly conserved from *Caenorhabditis elegans* to mammals, and has been primarily associated with the regulation of apicobasal polarity, but also plays a role in cell proliferation, cell migration, and planar-cell polarity and as a tumor suppressor (Elsum et al., 2012). Originally identified in *Drosophila melanogaster*, the Scribble complex comprises three proteins: Scribble, Discs large (Dlg), and lethal giant larvae (Lgl; Gateff and Schneiderman, 1974; Mechler et al., 1985; Woods and Bryant, 1991; Bilder and Perrimon, 2000). Mutations in each of these proteins result in loss of apico-basal polarity and uncontrolled proliferation, suggesting that Scribble, Dlg, and Lgl function in a common pathway (Bilder and Perrimon, 2000). Surprisingly, little evidence is available regarding the molecular mechanisms that control the function of the Scribble complex. Most information to date originates from genetic studies in flies, or loss of function experiments in mammals (Elsum et al., 2012). In mammalian cells, the Scribble complex has also been shown to play a role in adhesion and polarity, although the loss of function phenotypes described tend to be less pronounced than in *Drosophila* (Bonello and Peifer, 2018). Both Scribble and Dlg1 play a role in stabilizing E-cadherin at cell junctions (Laprise et al., 2004; Qin et al., 2005; Lohia et al., 2012), and silencing the expression of either Scribble or Dlg1 delays the formation of junctions and impairs the formation of single lumen, polarized

[1]Department of Biological Sciences, The University of Toledo, Toledo, OH; [2]Department of Molecular, Cellular, and Developmental Biology, University of Michigan, Ann Arbor, MI; [3]Department of Biochemistry, University of Iowa, Iowa City, IA; [4]International Center for Genetic Engineering and Biotechnology, Trieste, Italy.

Correspondence to Rafael Garcia-Mata: rafael.garciamata@utoledo.edu.

3D cysts (Laprise et al., 2004; Qin et al., 2005; Lohia et al., 2012; Awad et al., 2013; Yates et al., 2013; Hendrick et al., 2016).

The members of the Scribble complex are known to work as a functional module, where the function of each protein in the complex depends on the function of the others. However, very little is known about how the proteins in the Scribble complex—Scribble, Dlg, and Lgl—interact with each other, either physically or functionally, or which downstream signaling pathways are regulated by the Scribble complex.

Here, we show that Src homology 3 domain (SH3)–containing GEF (SGEF), a RhoG-specific GEF, interacts simultaneously with Scribble and Dlg1 and functions as a bridge that mediates the formation of a ternary complex. We use two complementary model systems, mammalian MCDK cells and *Xenopus laevis* embryos, to characterize the role of the Scribble/SGEF/Dlg1 ternary complex in the assembly and maintenance of cell–cell junctions, the regulation of apical contractility, and the establishment of apicobasal polarity both in 2D and 3D. Our results define two distinct roles for SGEF, a nucleotide exchange–dependent function, which regulates the assembly and maintenance of adherens junctions (AJs), and a scaffolding function that acts independent of catalytic activity, which regulates barrier function and apical contractility.

Results

SGEF interacts with Scribble through an internal PSD95, Dlg1, and ZO-1 family domain (PDZ)–binding motif (PBM)

We performed a yeast two-hybrid screen to identify proteins that interact with SGEF and identified Scribble as a potential binding partner for SGEF (Fig. S1 A). We then confirmed the interaction by coimmunoprecipitation and Western blot (WB) analysis in HEK293 cells expressing myc-SGEF WT and GFP-Scribble WT (Fig. 1, A and B). Since SGEF encodes a C-terminal PBM (García-Mata and Burridge, 2007; Fig. 1 A), we hypothesized that the PBM in SGEF was interacting with one of the four PDZ domains encoded in Scribble (Fig. 1 A). Our results confirmed that the interaction was mediated by the PDZ domains in Scribble, as deletion of the four PDZ domains (ΔPDZ) abolished the interaction (Fig. 1 C). In contrast, a Scribble mutant in which the N-terminal leucine-rich repeats region is not functional (P305L; Legouis et al., 2003) interacted efficiently with SGEF (Fig. 1 C). To map which of Scribble's PDZ domains mediated the interaction with SGEF, we tested the interaction between myc-SGEF and a series of Scribble constructs comprising either the four WT PDZ domains (4PDZ) or mutants in which each of the individual PDZ domains was inactivated by a mutation in its carboxylate binding loop (M1–M4; Petit et al., 2005). Our results showed that inactivation of PDZ1 in Scribble, but not the other PDZ domains, completely abolished the interaction with SGEF, suggesting the interaction is mainly mediated by PDZ1 (Fig. 1 D).

Surprisingly, the deletion of the PBM in SGEF (ΔETNV) had no effect on the ability of SGEF to bind to Scribble (Fig. 1 E). These results showed that SGEF's PBM was dispensable for its interaction with Scribble's PDZ domains and suggested that the interaction was mediated by an internal PBM (iPBM) in SGEF. To map the Scribble binding site in SGEF, we generated a series of deletion mutants in SGEF and analyzed their ability to interact with Scribble using coimmunoprecipitation. Our results showed that a construct comprising aa 228–871 of SGEF, which includes the PBM, was unable to bind, whereas a construct comprising the first 227 aa (SGEF 1–227) was sufficient to interact with Scribble (Fig. 1 F). Further deletion analysis narrowed down the Scribble-binding domain in SGEF to a region comprising aa 25–50 (Fig. 1 G). Alanine scanning mutagenesis of selected amino acids within this region led to defining the minimal region required for binding to residues S39–E54, a region that is highly conserved in vertebrates (Fig. 1, H and I). When amino acids LITD or FPVE were substituted by alanine, the interaction between SGEF and Scribble was completely abolished (Fig. 1 I), suggesting that this region is part of the binding motif. Mutation of SYQS, located upstream of LITD, had minimal effect, whereas mutating RSKP residues further upstream had no effect on binding. Interestingly, substitution of VED, which overlaps partially with FPVE, restored binding, although not completely (Fig. 1 I). In addition, a single amino acid substitution in Thr 49 (T49A) within the LITD motif was sufficient to completely abolish the interaction (Fig. S1 B). Replacing the upstream Gly 45 residue for Pro also abolished the interaction (Fig. S1 B). Taken together, our results show that the sequence comprising residues LITDFP within the N terminus of SGEF is essential for binding Scribble, and some of the residues located immediately upstream and downstream may also contribute to the interaction.

The structure of Scribble PDZ1/SGEF-PDZ$_{peptide}$ complex

To obtain insight into the atomic details of the Scribble PDZ1/SGEF interaction, we sought to determine the x-ray crystal structure of the complex between Scribble PDZ1 and a peptide encoding the SGEF amino acids KPNGLLITDFP (Fig. 1 I). We obtained high-quality protein samples that yielded crystals. Crystals of the apo PDZ1 domain diffracted to a resolution of 1.6 Å, and we determined the structure using routine methods. The Scribble PDZ1 in complex with SGEF-PDZ$_{peptide}$ also yielded crystals. Crystals of the Scribble PDZ1 domain in complex with the SGEF-PDZ$_{peptide}$ peptide diffracted to a resolution of 1.1 Å. Using molecular replacement and the apo PDZ1 structure as search model, we solved the structure of the complex. Table S3 summarizes the crystallographic data and refinement statistics. A comparison of the structures for the apo Scribble PDZ1 domain and the PDZ1/SGEF-PDZ$_{peptide}$ complex is shown in Fig. 1 J. The electron density of the SGEF peptide shows the high quality of the data and the ability to unambiguously trace the conformation of the peptide. This structure revealed several unique features of the Scribble PDZ1/SGEF interaction where SGEF's PBM is located internally, compared with typical PDZ interactions with C-terminal PBM. First, 11 residues of SGEF-PDZ$_{peptide}$ make interactions with the Scribble PDZ domain covering ∼500 Å^2 of accessible surface area. For context, analyses of several typical PDZ/C-terminal complexes with ligands of five to six residues encompass ∼350 Å^2 of accessible surface area (Liu et al., 2013; Ren et al., 2015; Raman et al., 2016; Lim et al., 2017). Second, the structure revealed the register of the peptide with respect to the

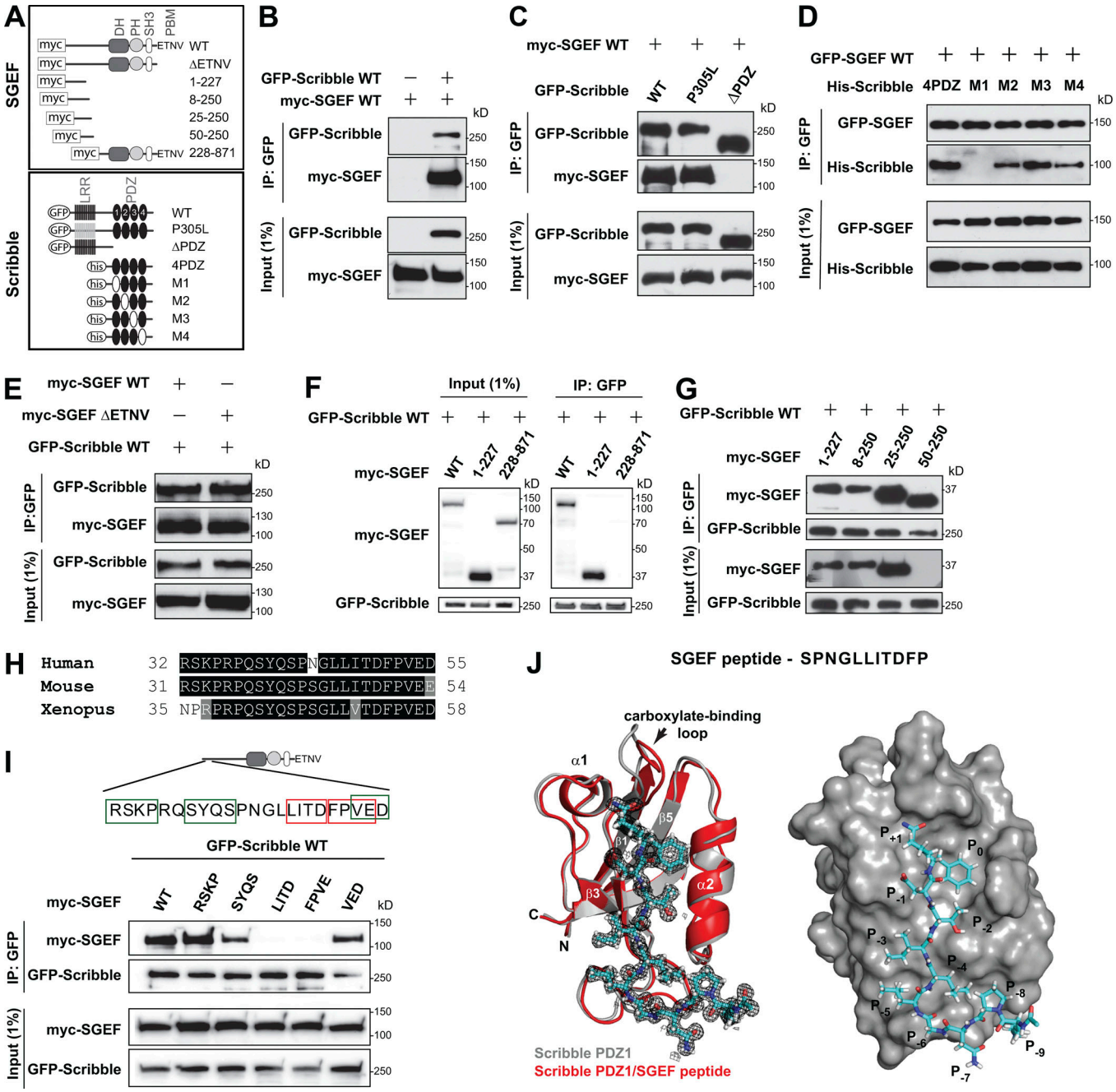

Figure 1. **SGEF interacts with Scribble PDZ domain through a novel PBM. (A)** Schematic representation of SGEF and Scribble constructs used in this figure. LRR, leucine-rich repeat. **(B–G)** Lysates from HEK293FT cells expressing the indicated constructs were immunoprecipitated (IP) using GFP antibodies (GFP-trap nanobodies). In all experiments, the precipitates were immunoblotted with anti-GFP antibodies to detect the immunoprecipitated protein and with anti-myc or anti-His to detect the potential interacting partner. **(H)** Sequence alignment comprising the Scribble binding domain of SGEF in vertebrates (aa 32–55 in human). **(I)** The indicated boxed regions within the Scribble binding domain in SGEF were mutagenized to Ala in full-length SGEF. Lysates from HEK293FT cells expressing the myc-tagged WT-SGEF or the indicated Ala mutants and GFP-Scribble were immunoprecipitated using GFP antibodies (GFP-trap nanobodies). The precipitates were immunoblotted with anti-GFP antibodies to detect the immunoprecipitated protein and with anti-myc to detect my-tagged SGEF mutants. Green boxes show the sequence that when mutated still maintain an interaction with Scribble whereas the red boxes denote sequence that when mutated lead to loss of interaction with Scribble. **(J)** Crystal structure of the Scribble PDZ1 domain in complex with an SGEF iPBM peptide. The crystal structure of the apo Scribble PDZ1 domain is shown in gray, while the complex with the $SGEF_{peptide}$ (KSPNGLLITDFP) is shown in red (left panel). The right panel is a surface representation of the PDZ1/SGEF-$PDZ_{peptide}$ complex.

PDZ domain, such that the P_0 Phe and P_{-2} Thr in SGEF occupy the canonical S_0 and S_{-1} pockets in Scribble PDZ1. Importantly, the structure revealed several novel interactions through pockets near the α1 helix in Scribble PDZ1 (S_{+1} pocket), which accommodate the P_{+1} Pro in SGEF (Fig. 1 J). These features are distinct from the two published PDZ/internal ligand structures (Hillier et al., 1999; Penkert et al., 2004).

SGEF's N-terminal region interacts with the guanylate kinase (GUK) domain of Dlg1

Our previous work has shown that SGEF also interacts with Dlg1, which is a member of the canonical Scribble polarity complex (Krishna Subbaiah et al., 2012). The interaction between SGEF and Dlg1 was reported to involve SGEF's PBM binding to PDZ domains 1 and 2 of Dlg1, and an additional interaction between the SH3 domains of both SGEF and Dlg1 (Krishna Subbaiah et al., 2012). The fact that SGEF's binding site for Scribble does not overlap with the binding site for Dlg1 raises the possibility that SGEF interacts simultaneously with both Scribble and Dlg1. To confirm the interaction between SGEF and Dlg1 and map the Dlg1 binding site in SGEF, we took advantage of tools and approaches similar to those used in Fig. 1. As expected, both SGEF WT and SGEF 228–871, which contains the DH-PH domains, the SH3 domain, and the PBM, were able to bind efficiently to Dlg1 (Fig. 2, A and B). SGEF 1–227, which binds to Scribble, did not interact with Dlg1 (Fig. 2 B). To explore the SGEF/Dlg1 interaction in more detail, we deleted either the PBM (SGEF ΔETNV) or both the PBM and the SH3 domain (SGEF ΔSH3) in SGEF and tested their ability to bind Dlg1. We expected that upon deletion of these two domains, the interaction between SGEF and Dlg1 would be abolished. Surprisingly, both mutants still interacted efficiently with Dlg1 (Fig. 2 C). Since this result was contrary to what had been previously published (Krishna Subbaiah et al., 2012), we conducted additional experiments to confirm or disprove these findings. We first designed two truncation mutants of SGEF and tested them for Dlg1 binding, one encoding the N-terminal half that ends just before the start of the DH-PH domain (1–414) and the other encoding the C-terminal half, which includes the DH-PH domain, the SH3 domain, and the PBM (414–871) (Fig. 2 A). The N-terminal half of SGEF (1–414) interacted efficiently with Dlg1, whereas the C-terminal half (414–871) showed no binding (Fig. 2 D). Together, these results suggested that the binding site for Dlg1 lies between aa 227–414 in SGEF (Fig. 2, B and D). To further narrow down the binding site, we tested a series of SGEF deletion mutants covering the region between aa 300–400. Our results showed that SGEF 1–350 and 1–400 were able to bind to Dlg1, whereas SGEF 1–300 was not, suggesting that the region between aa 300–350 of SGEF was required for binding Dlg1 (Fig. 2 D, right panel). This region of SGEF exhibits no conserved structural domains but is highly conserved in vertebrates (Fig. 2 G). In addition, it does not encode any obvious PBM, suggesting that the SGEF-binding site in Dlg1 is not located within the PDZ domains of Dlg1.

To map the SGEF-binding domain in Dlg1, we first tested the interaction between SGEF WT and two Dlg1 constructs, one encoding the N-terminal half including the three PDZ domains, and the other one the C-terminal half comprising the SH3 and GUK domains (Fig. 2 A). Interestingly, the Dlg1 N terminus showed no detectable binding to SGEF, confirming that the PDZ domains of Dlg1 were not involved in the interaction (Fig. 2 E). In contrast, the Dlg1 C-terminal construct was able to bind efficiently to SGEF (Fig. 2 E). We confirmed these results using a Dlg1 mutant construct in which the three PDZ domains were inactivated by mutations. Our results showed that inactivating the PDZ domains abolished a previously described interaction with the RhoA GEF Net1 (García-Mata et al., 2007), but had no effect on the ability of Dlg1 to bind to SGEF (Fig. S1 C). We then used a series of truncation mutants to further define the SGEF-binding domain in Dlg1. Deleting the GUK domain in Dlg1 abolished the interaction with SGEF, and the GUK domain alone was able to interact with SGEF (Fig. 2 F). In contrast, the SH3 domain by itself showed no detectable binding (Fig. 2 F). Overall, our results demonstrate that the PDZ and SH3 domains in Dlg1 are not required to bind to SGEF as previously reported, but instead reveal that the GUK domain of Dlg1 interacts with a conserved 50-aa region at the N terminus of SGEF (Fig. 2 G).

SGEF forms a ternary complex with Scribble and Dlg1

Our data demonstrates that Scribble and Dlg1 interact with distinct regions in SGEF (Fig. 1 and Fig. 2), suggesting that SGEF could bind simultaneously to Scribble and Dlg1, forming a ternary complex. To test this possibility, we coexpressed HA-Scribble and GFP-Dlg1 in HEK293 cells in the presence or absence of myc-SGEF. We then immunoprecipitated Dlg1 using anti-GFP antibodies and immunoblotted for the three proteins. We predicted that if SGEF forms a ternary complex with Scribble and Dlg1, Scribble would coprecipitate with Dlg1 only when SGEF is present. Indeed, Scribble did not coprecipitate with Dlg1 in the absence of SGEF; however, when the three proteins were coexpressed, Scribble coprecipitated efficiently with Dlg1, demonstrating that the three proteins form a ternary complex (Fig. 3 A). Using a similar coprecipitation approach, we then confirmed the existence of the endogenous Scribble/SGEF/Dlg1 ternary complex in human epithelial cells (Caco-2; Fig. 3 B) and in MDCK cells (Fig. 3 C). When the expression of SGEF is silenced in MDCK cells, Scribble fails to coprecipitate with Dlg1, confirming that SGEF is required for the formation of the endogenous ternary complex (Fig. 3 C). We also determined that the minimum SGEF mutant that can mediate the formation of the Scribble/SGEF/Dlg1 complex (SGEF 1–414) must contain both the Scribble and Dlg1 binding sites (Fig. 3, D and E), consistent with the data presented in Fig. 1 and Fig. 2. Deletion of either the Scribble iPBM or the Dlg1 binding motif in SGEF abolished the formation of the complex (Fig. 3, D and E). Overall, our results demonstrate that the interaction between SGEF/Scribble and SGEF/Dlg1 can occur simultaneously, allowing for the formation of a ternary complex between Scribble, SGEF, and Dlg1 (Fig. 3 F).

SGEF localizes at cell–cell junctions in epithelial cells

To investigate the functional role of the Scribble/SGEF/Dlg1 ternary complex, we used two complementary model systems: (1) MDCK cells (MDCK II), which are the preferred mammalian model to study junction formation and polarity (Rodriguez-Boulan and Macara, 2014), and (2) *Xenopus* embryos, which provide an ideal system to study cell–cell junctions and cell polarity in an intact epithelial environment during development (Woolner et al., 2009; Blum et al., 2015; Stephenson and Miller, 2017). The SGEF sequence is highly conserved in vertebrates, allowing us to use the information gained from biochemical and mammalian cell culture systems to guide experiments in *Xenopus* embryos.

To investigate the localization of SGEF, we expressed low levels of human mNeon-SGEF WT in MDCK cells and compared

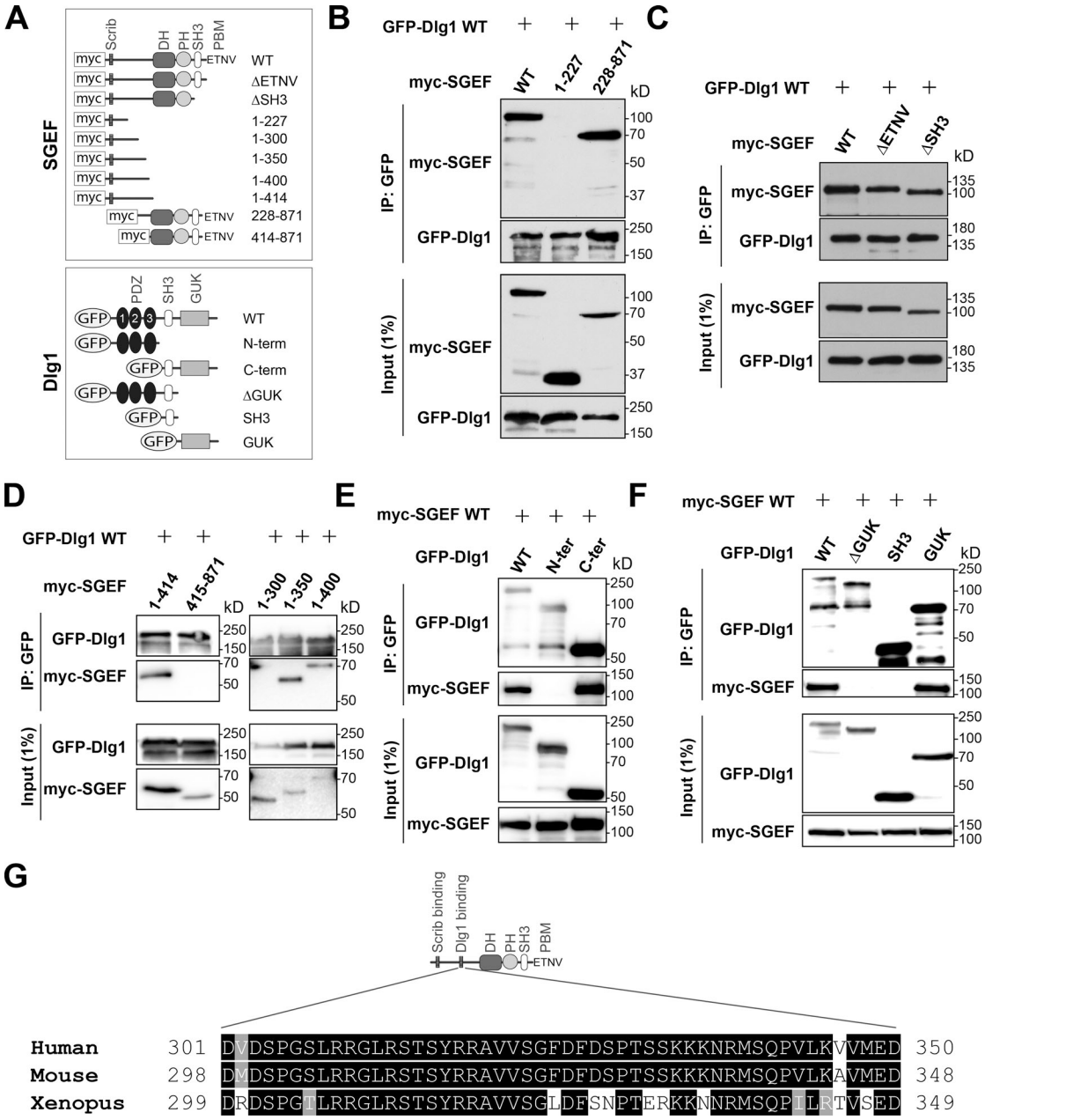

Figure 2. **SGEF's N terminus interacts with Dlg1 GUK domain. (A)** Schematic representation of SGEF and Dlg1 constructs used in this study. **(B–F)** Lysates from HEK293FT cells expressing the indicated constructs were immunoprecipitated using GFP antibodies (GFP-trap nanobodies). In all experiments, the precipitates were immunoblotted with anti-GFP antibodies to detect the immunoprecipitated protein and with anti-myc to detect the interacting partner. **(G)** Sequence alignment comprising the Dlg1 binding domain of SGEF in vertebrates (aa 301–350 for human).

its localization to that of endogenous Scribble and Dlg1. Both Scribble and Dlg1 are distributed throughout the lateral membrane in epithelial cells, where they colocalize with AJ and tight junction (TJ) markers (Dow et al., 2003; Laprise et al., 2004; Navarro et al., 2005; Ivanov et al., 2010). As expected from our protein interaction studies (Figs. 1, 2, and 3), mNeon-SGEF WT colocalized with both Scribble and Dlg1 (Fig. 4 A). Indeed, mNeon-SGEF WT localized to the apical junctional complex (AJC; Farquhar and Palade, 1963), colocalizing with markers for both TJs (ZO-1) and AJs (β-catenin; Fig. 4 B). Endogenous SGEF also targets to junctions in MDCK cells, where it colocalizes with Scribble (Fig. S2 A).

In addition, mNeon-SGEF WT targeted very efficiently to the AJC in gastrula-stage (stage 10.5–12; Nieuwkoop and Faber, 1994) *Xenopus* embryos, where it colocalized with both TJ (BFP-ZO-1) and AJ (PLEKHA7-mCherry) markers (Fig. 4 C). Reconstructed XZ planes of these images demonstrated that SGEF signal is distributed along the lateral membrane, with the bulk of the signal concentrated at the apical region, overlapping slightly better with BFP-ZO-1 (TJ) than with mCherry-PLEKHA7 (AJ; Fig. 4, C and C′). SGEF's apical localization was better defined in *Xenopus* compared with MDCK cells, where mNeon-SGEF WT signal was distributed more evenly along the lateral membrane (Fig. 4, A and B).

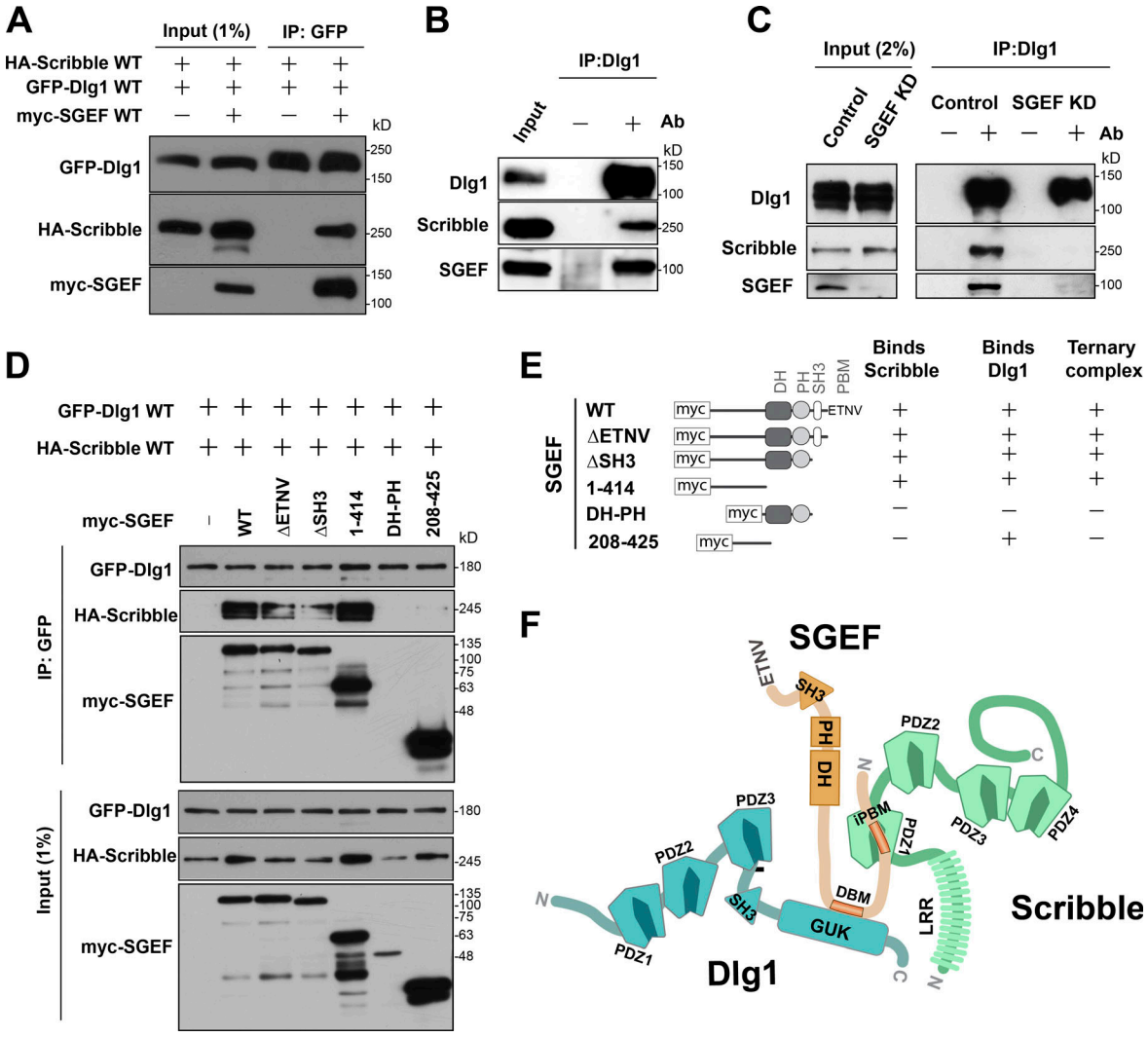

Figure 3. **SGEF forms a ternary complex with Scribble and Dlg1. (A)** Lysates from HEK293FT cells expressing GFP-Dlg1 and HA-Scribble in the presence or absence of myc-SGEF were immunoprecipitated using GFP antibodies (GFP-trap nanobodies). The precipitates were immunoblotted with anti-myc, anti-GFP, and anti-HA antibodies as indicated. **(B)** Endogenous Dlg1 was immunoprecipitated from Caco2 cell lysates and immunoblotted for Dlg1, SGEF, and Scribble. **(C)** Endogenous Dlg1 was immunoprecipitated from CTRL and SGEF KD MDCK cell lysates and immunoblotted for Dlg1, SGEF, and Scribble. **(D)** Lysates from HEK293FT cells expressing the indicated constructs were immunoprecipitated using GFP antibodies (GFP-trap nanobodies). The precipitates were immunoblotted with anti-GFP antibodies to detect the immunoprecipitated protein and with anti-myc and anti-HA to detect the interacting partners. **(E)** Summary of results from C. **(F)** Cartoon representation of the ternary complex between Scribble, SGEF, and Dlg1. DBM, Dlg binding motif; iPBM, internal PDZ-binding motif.

Since SGEF is a GEF specific for the small GTPase RhoG, we expressed mNeon-RhoG to determine if it was also targeted to cell–cell junctions. We found that indeed, RhoG colocalized with TJ and AJ markers in both *Xenopus* embryos (Fig. 4 D) and MDCK cells (Fig. S2, B–E). However, compared with SGEF, which is strongly concentrated at apical junctions in *Xenopus* embryos (Fig. 4 C′), RhoG was more broadly localized along the lateral membrane (Fig. 4 D′).

To determine whether binding to Scribble and Dlg1 is important for targeting SGEF to the AJC, we compared the localization of mNeon-SGEF WT (SGEF WT) and two deletion mutants of SGEF—one that binds to Scribble but not to Dlg1 (SGEF 1–227) and another that binds to Dlg1 but not to Scribble (SGEF 228–871)—in *Xenopus* embryos. We found that both SGEF WT and SGEF 1–227 localized efficiently to the AJC, where they colocalized with ZO-1 (Fig. 4, E and F). In contrast, SGEF 228–871 was predominantly cytosolic, with only a small fraction still targeted to junctions (Fig. 4, E and F). Overall, our results suggested that binding to Scribble is the main determinant for SGEF to localize at the AJC.

SGEF knockdown (KD) down-regulates E-cadherin protein levels and affects AJ formation and architecture

To assess the functional role of SGEF during junction formation, barrier formation, and the establishment of cell polarity, we generated stable MDCK cells expressing a previously published shRNA sequence targeting SGEF (Qin et al., 2010). SGEF protein levels were significantly reduced in SGEF KD cells (Fig. 5 A). We

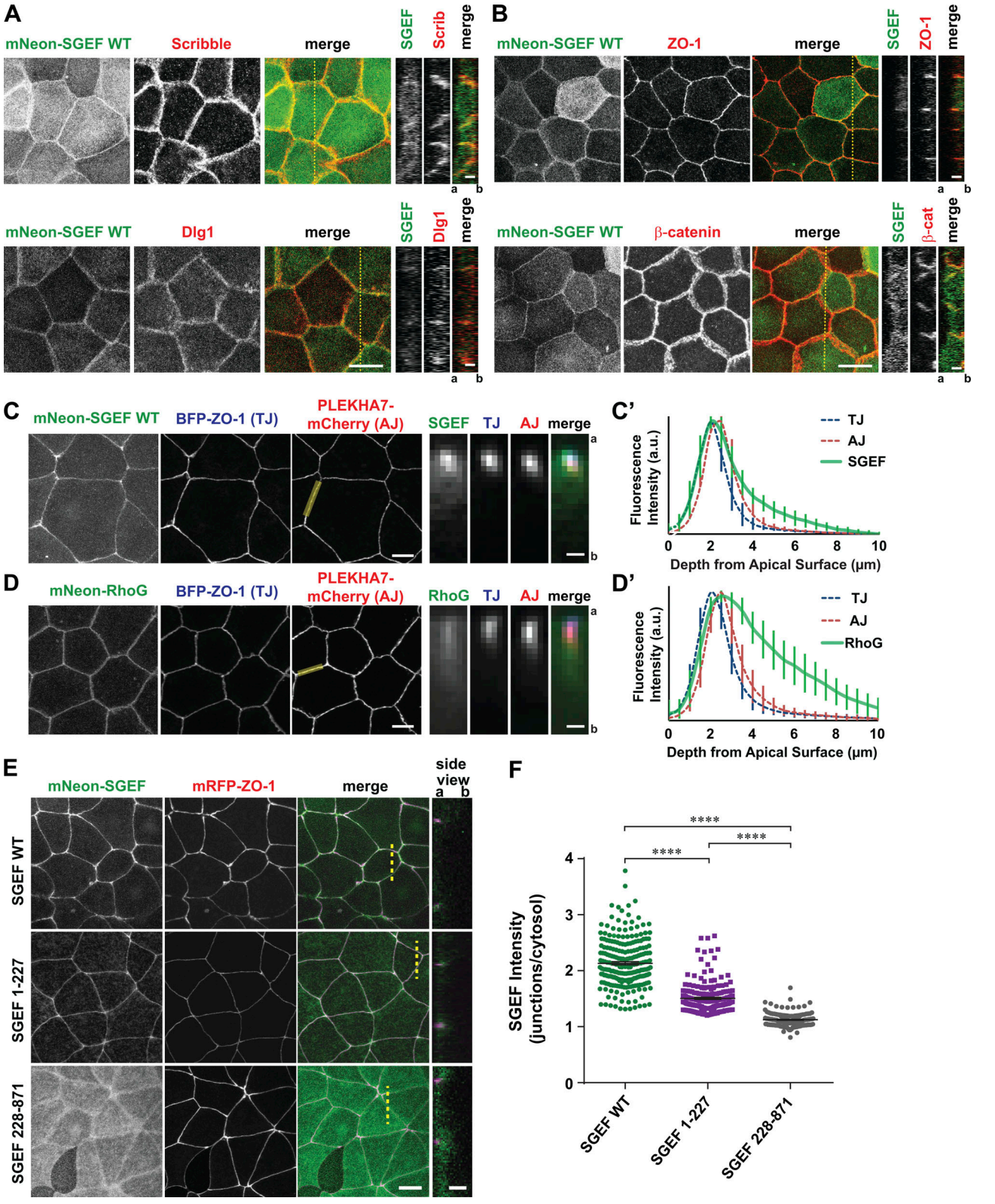

Figure 4. **SGEF localizes at cell–cell junctions in epithelial cells. (A and B)** IF of MDCK cells showing colocalization of mNeon-SGEF WT with Scribble and Dlg1, ZO-1 (TJ marker), and β-catenin (AJ marker). The right panels are single Z-planes along the length of the dotted yellow line. a, apical, b, basal. Scale bar, 10 µm, and XZ, 3 µm. **(C)** Gastrula-stage *Xenopus* embryos expressing mNeon-SGEF WT (green), TagBFP-ZO-1 (TJ marker), and PLEKHA7-mCherry (AJ marker) were live-imaged using confocal microscopy. En face views (left) are brightest point projections across multiple Z-planes. Side views (right) are average intensity projections along the length of the highlighted junction (see Materials and methods). Scale bars, XY, 10 µm, and XZ, 1 µm. **(C')** Intensity profiles of SGEF (green solid line) relative to AJs (red dotted line) and TJs (blue dotted line) along the z axis in *Xenopus* gastrula-stage epithelial cells. Note that SGEF's peak intensity is close to ZO-1's, but it tapers away more slowly than ZO-1 along the lateral membrane. The graph shows normalized averaged intensities fitted with

a smoothed curve; error bars indicate SD; *n* = 47 junctions, 18 embryos, five experiments. **(D)** Gastrula-stage *Xenopus* embryos expressing mNeon-RhoG (green), BFP-ZO-1 (TJ marker, blue), and PLEKHA7-mCherry (AJ marker, red) were live imaged using confocal microscopy. Brightest point projections of en face views and averaged side views of the highlighted junction (as in C) are shown. Scale bars, XY, 10 µm, and XZ, 1 µm. **(D′)** Intensity profiles of RhoG (green solid line) relative to AJs (red dotted line) and TJs (blue dotted line). Note that the RhoG signal is more basolateral compared with SGEF. The graph shows normalized averaged intensities fitted with a smoothed curve; error bars indicate SD. *n* = 19 junctions, 10 embryos, three experiments. **(E)** Gastrula-stage *Xenopus* embryos expressing mRFP-ZO-1 (TJ marker, magenta) and mNeon-SGEF WT (top, green), SGEF 1–227 (middle, green), or SGEF 228–871 (bottom, green) were live-imaged using confocal microscopy. En face views are brightest point projections across multiple Z-planes. Side views (right) are single Z-planes at the locations marked by yellow dotted lines. Note that WT SGEF and SGEF 1–227 appear junctional, whereas SGEF 228–871 appears diffusely localized. Scale bars, 20 µm, and XZ, 5 µm. **(F)** Quantification of the ratio of junctional to cytosolic intensities of mNeon-tagged SGEF WT, SGEF 1–227, and SGEF 228–871 in *Xenopus* embryos. *n* = SGEF WT: 234 junctions, 12 embryos, six experiments; SGEF 1–227: 214, 11, 5; SGEF 228–871: 180, 9, 4. Error bars represent SEM. ****, P < 0.00005 using the Mann–Whitney *U* test.

first analyzed the morphology of AJs in CTRL (expressing a nontargeting shRNA) and SGEF KD cells by immunofluorescence (IF) microscopy. Surprisingly, we found that silencing SGEF expression led to an almost complete loss of E-cadherin from the AJs (Fig. 5 C). This loss of E-cadherin at junctions was due to a decrease in E-cadherin protein levels, and not to its redistribution to different cellular locations (Fig. 5, B and C). Note that E-cadherin decrease was not uniform at different regions of the monolayer in SGEF KD cells, probably reflecting differences in KD efficiency in a stable SGEF KD mixed population. We also generated single cell SGEF KD colonies that showed a much more homogeneous degree of E-cadherin reduction when stained by IF (Fig. S2 F). Reexpression of human mNeon-SGEF WT in SGEF KD MDCK cells (Rescue WT) restored both the proper expression level and localization of E-cadherin (Fig. 5, B, C, and G). Since the cytoplasmic tail of E-cadherin binds to β-catenin and p120-catenin, we also analyzed their expression levels and localization. Interestingly, the protein levels of β-catenin and p120-catenin were not affected in SGEF KD cells (Fig. 5 B), but their localization at cell–cell junctions was disorganized compared with the CTRL cells (Fig. 5, C′, D, and G). The localization of both β-catenin and p120-catenin to cell–cell junctions was restored to normal in Rescue WT cells (Fig. 5, C′, D, and G). The fact that some markers such as p120-catenin and β-catenin, although disorganized, were still present at cell junctions even in the absence of E-cadherin suggested that there might be other cadherins compensating for the loss of E-cadherin. Using a pan-cadherin antibody, which recognizes most type I and II cadherins, we found that the combined expression levels of cadherins were not obviously changed in SGEF KD cells (Fig. 5 B). This indicated that one or more of the classical cadherins were up-regulated in response to the loss of E-cadherin. A potential candidate is cadherin-6 (K-cadherin), which is expressed in MDCK cells and is up-regulated in confluent cells (Stewart et al., 2000). WB analysis showed that in SGEF KD cells, the loss of E-cadherin was accompanied by a subsequent increase in cadherin-6 levels, which were restored to normal levels when SGEF expression was rescued (Fig. 5 B).

To determine whether binding to SGEF plays a role in targeting the Scribble complex to junctions and/or regulating its stability, we also analyzed the effects of silencing SGEF on the expression levels and localization of Scribble and Dlg1. WB analysis showed that the expression levels of Scribble and Dlg1 were not affected in SGEF KD cells (Fig. 5 B). In contrast, immunostaining for endogenous Scribble and Dlg1 showed that in SGEF KD cells, the localization of Scribble was slightly more diffuse than in CTRL cells, whereas Dlg1 showed a more severe phenotype with a highly disorganized pattern at junctions (Fig. 5, E–G). Quantification shows that, even though both Scribble and Dlg1 showed a more diffuse pattern in SGEF KD cells, Dlg1 showed a larger decrease in the intensity peak at the junctions when compared with Scribble (Fig. 5 G). Rescue with mNeon-SGEF WT restored the normal localization of both Scribble and Dlg1 (Fig. 5, E–G). As shown in Fig. 4, E and F, Scribble is important for recruiting SGEF to junctions, so silencing SGEF is not expected to affect Scribble localization. Taken together, these results suggest that SGEF is important for targeting Dlg1. The small effect observed on Scribble localization may indicate a role for SGEF in targeting/stabilizing Scribble or might be an indirect consequence of the effects of SGEF KD on AJ structure (Fig. 5, C and D).

The absence of E-cadherin in SGEF KD cells may compromise the ability of cells to assemble the lateral membrane, which has lipids and proteins distinct from the apical and basal membranes and thus is compositionally and functionally distinct. The lateral membrane plays a key role in providing mechanical stability to epithelial cells (Tang, 2017). To determine whether the loss of E-cadherin observed upon silencing SGEF was affecting the structure of the lateral membrane, we analyzed confocal XZ images from CTRL, SGEF KD, and Rescue WT cells stained for E-cadherin and β-catenin (Fig. 5 H). Interestingly, silencing SGEF had a striking effect on the height of the monolayer, which was significantly decreased. Quantification showed that CTRL cells averaged 5.94 ± 0.18 µm in height, whereas SGEF KD cells had an average height of 2.50 ± 0.02 µm. Rescue with mNeon-SGEF WT restored the cell height to normal levels with an average height of 5.61 ± 0.16 µm (Fig. 5 I). These results suggest that the loss of E-cadherin in SGEF KD cells may prevent the cells in the monolayer from establishing their normal cuboidal shape.

To determine whether SGEF KD also affects the establishment of junctions, we performed a calcium switch assay. In this assay, cell–cell junctions are disrupted when cells are grown in the absence of Ca^{2+}, due to the loss of Ca^{2+}-dependent cadherin-mediated adhesion. Subsequent restoration of physiological levels of Ca^{2+} results in the synchronous de novo assembly of cell–cell junctions (Cereijido et al., 1978; Gumbiner and Simons, 1986). Our results revealed that 2 h after replenishing calcium to the medium, CTRL cells had already established visible AJs and TJs. In contrast, the formation of AJs and TJs in SGEF KD cells was significantly delayed (Fig. S3), taking ≥6 h to establish comparable AJs and TJs.

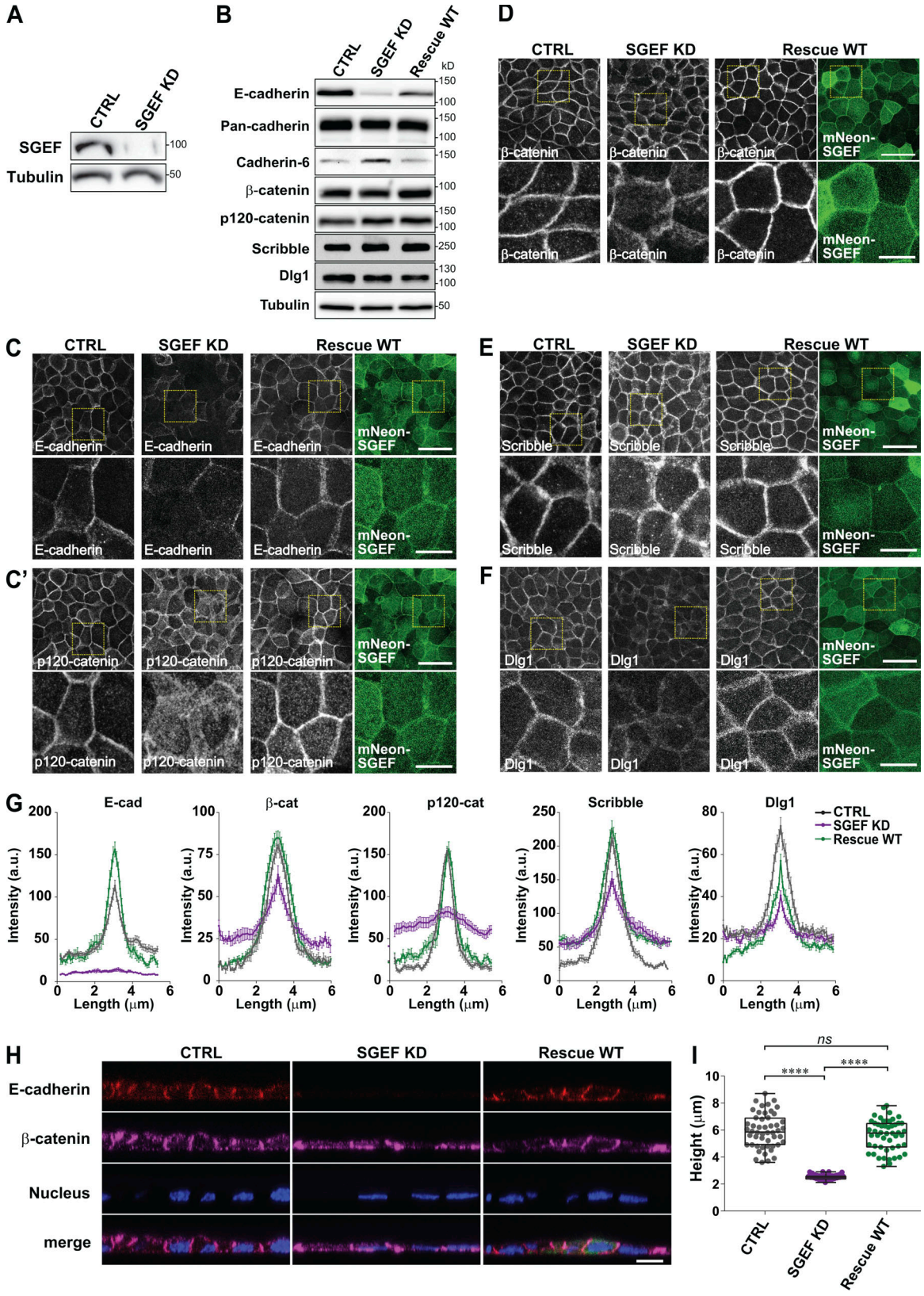

Figure 5. **SGEF regulates AJ properties of epithelial cells. (A)** Cell lysates from confluent CTRL and SGEF KD MDCK cells were analyzed by WB using anti-SGEF antibodies. Tubulin was used as a loading control. **(B)** Cell lysates from confluent CTRL, SGEF KD, and Rescue WT MDCK cells were probed with E-cadherin, Pan-cadherin, cadherin-6, β-catenin, p120-catenin, Scribble, and Dlg1 antibodies. Tubulin was used as a loading control. **(C, C′, and D–F)** IF showing the distribution of endogenous E-cadherin, p120-catenin, Scribble, Dlg1, β-catenin, and mNeon-SGEF (green) in CTRL, SGEF KD, and Rescue WT MDCK cells. The bottom panel in each set of images shows a zoomed image of the selected regions (dotted yellow line). Note that panels C and C′ show images from

same field. Confocal images are maximum projections of apical Z-planes. Scale bars, top panels: 30 µm; bottom panels: 10 µm. **(G)** Linescan (6-µm line drawn perpendicular to center of junctions) of IF images in panels C to F. At least two fields from two independent experiments were used for quantification (≥200 junctions). The intensity profiles were manually centered around the highest peak for each condition. **(H)** XZ view of MDCK cells from CTRL, SGEF KD, and Rescue WT cells stained for E-cadherin (red), β-catenin (magenta), nucleus (blue) and mNeon-SGEF WT (green in merge panel). Scale bar, 10 µm. **(I)** Quantification of height in CTRL, SGEF KD, and Rescue MDCK cells. $n = 50$ cells for each condition from three independent experiments. Error bars represent min to max with all points. ****, $P < 0.00005$; *ns*, nonsignificant using Student's *t* test (two-tailed, unpaired).

Taken together, our results suggest that SGEF regulates the formation and maintenance of cadherin-based AJ through the regulation of E-cadherin expression levels. In the absence of SGEF, the E-cadherin protein level is strongly reduced, AJ components are disorganized, and the lateral membrane collapses. Cadherin-6 up-regulation appears to compensate somewhat for the reduction in E-cadherin in SGEF KD cells and helps to maintain cell–cell adhesion and the integrity of the monolayer, although it might not be sufficient to functionally replace the loss of E-cadherin, as AJs remain disorganized.

SGEF KD changes TJ morphology and reduces barrier function

It has been previously shown that the assembly of AJs leads to the formation of TJs and that interfering with AJ formation affects the structure and function of TJs (Gumbiner et al., 1988; Watabe et al., 1994; Tunggal et al., 2005). Since our results indicated that SGEF regulates the formation and maintenance of AJs, we then investigated whether SGEF was also required for TJ organization. We first examined the effect of silencing SGEF on the distribution of the TJ marker ZO-1. Our results revealed that SGEF depletion had a significant effect in the morphology of TJs. In MDCK cells, TJs typically adopt a characteristic curvilinear/zigzag pattern (Stevenson et al., 1988), as shown for CTRL cells (Fig. 6 A). In SGEF KD cells, however, TJs adopted a much more linear configuration, with most TJs appearing as a straight line (Fig. 6 A). The degree of linearity displayed by TJs can be calculated using the zigzag index, which is defined as the ratio of the length of a freehand line traced along the shape of a TJ from cell vertex to vertex to that of a straight line drawn from cell vertex to vertex (Tokuda et al., 2014). A zigzag index of 1 would indicate a straight line. The average zigzag index decreased from 1.24 in CTRL cells to 1.03 in SGEF KD cells. Reexpression of mNeon-SGEF WT in SGEF KD cells restored the normal curvilinear pattern of TJ, and the zigzag index increased significantly to 1.16 (Fig. 6, A and B). In addition to exhibiting straight TJs, SGEF KD cells displayed a more uniform apical area and isometric shape when compared with CTRL cells (Fig. 6 A). This was confirmed by measuring the apical area, which showed a small but significant increase in SGEF KD cells (Fig. 6 C). Furthermore, the apical area measurements for individual SGEF KD cells were distributed within a narrower range when compared with CTRL and Rescue WT cells, which indicates a more uniform size (Fig. 6 C). In addition, the axial ratio (major/minor axis aspect ratio) also decreased significantly when SGEF was silenced, indicating that SGEF KD cells exhibit a more isometric shape (Fig. 6 D), which could be rescued by reexpressing mNeon-SGEF WT (Fig. 6 D). We next determined whether the alterations observed in TJ architecture affected paracellular permeability by analyzing the transepithelial electrical resistance (TEER), which measures the charge-selective permeability of small solutes in confluent monolayers grown on semi-permeable filters (Shen et al., 2011) and provides an indication of TJ barrier function (Anderson and Van Itallie, 2009). We measured TEER in confluent CTRL, SGEF KD, and Rescue WT MDCK cells, and found that TEER was significantly reduced in SGEF KD cells compared with CTRL and Rescue WT cells (Fig. 6 E). Taken together, these results suggest that SGEF regulates the architecture of TJs, which affects both the size and shape of epithelial cells, as well as their barrier function.

SGEF KD stimulates actomyosin contractility at cell–cell junctions

The straight TJ phenotype displayed by SGEF KD cells bears a striking resemblance to the phenotype induced by silencing ZO-1 and ZO-2 (Fanning et al., 2012; Choi et al., 2016). Silencing ZO-1 and ZO-2 promotes the assembly of a highly organized actomyosin array at the AJC, which results in an increase in the tension at the junctions (Fanning et al., 2012; Choi et al., 2016). We found that in SGEF KD cells, myosin IIB was also arranged periodically in apical arrays adjacent to the apical cell–cell junction (Fig. 7 A). In contrast, CTRL and Rescue WT cells showed a more diffuse myosin IIB pattern that was only weakly associated with junctions (Fig. 7 A). To further characterize the actomyosin arrangement at junctions, we stained the cells for F-actin and myosin IIB and imaged them using HyVolution super-resolution technology. In CTRL cells, very little myosin IIB can be found colocalizing with actin at bicellular junctions (BCJ), but at tricellular junctions (TCJ) the signal is more concentrated, as has been previously shown (Fig. 7 B, white arrowheads; Fanning et al., 2012). In contrast, SGEF KD cells show an enlarged actomyosin array with myosin IIB distributed periodically along both sides of the BCJ (Fig. 7 B, yellow arrowhead). In addition, silencing SGEF promoted a dramatic increase in the number and thickness of stress fibers at the basal side of the cell, something that was not observed in ZO-1/2 double KD cells (Fanning et al., 2012; Choi et al., 2016). These stress fibers were also abundantly decorated with myosin IIB when compared with those in CTRL cells (Fig. 7 B and Fig. S4). Reexpression of mNeon-SGEF WT in SGEF KD cells restored the normal apical and basal actomyosin pattern (Fig. 7 B).

We did not observe a significant difference in the protein expression levels of myosin IIB in SGEF KD cells, suggesting that the phenotype observed was mainly driven by increased myosin rearrangement (Fig. 7 D). Treatment with either the myosin inhibitor blebbistatin or the ROCK inhibitor Y-27632 disrupted the apical actomyosin array, as well as the basal stress fibers (Fig. S4, A and A′), although blebbistatin had a stronger effect than Y-27632. This could be due to the fact that cells were treated

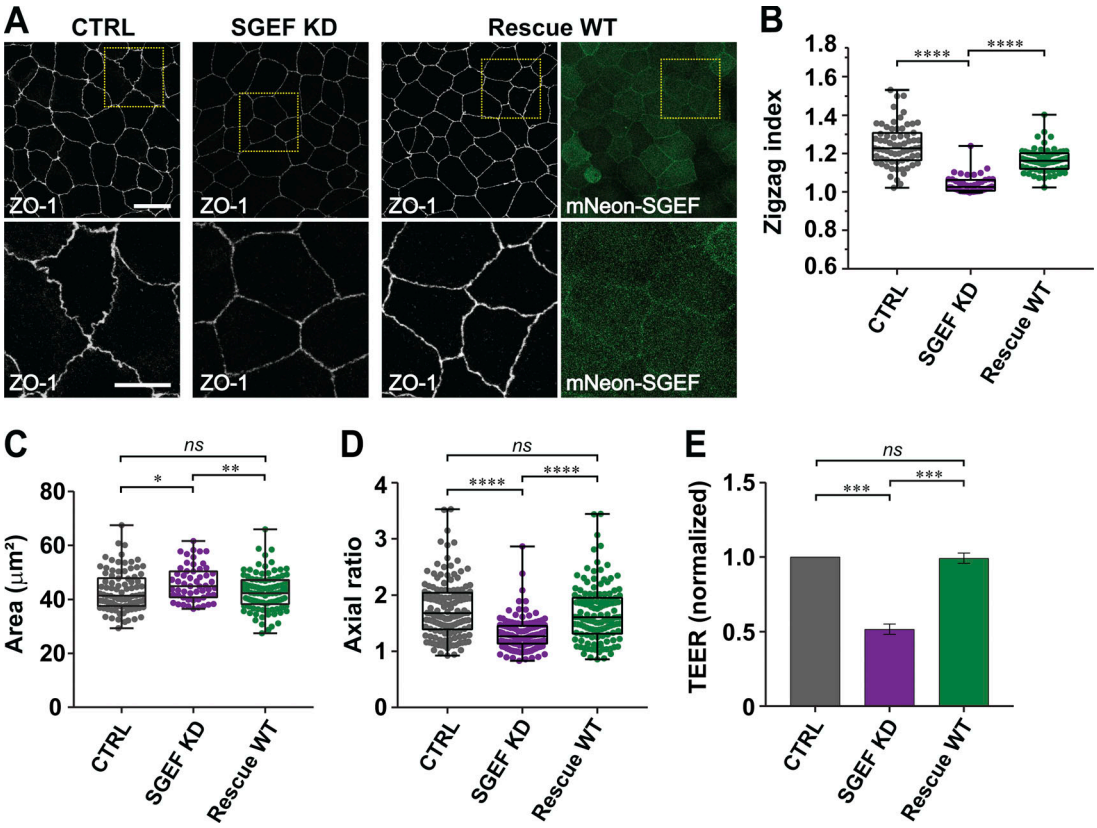

Figure 6. **SGEF KD regulates TJ architecture and permeability. (A)** Confocal images showing maximum projection of apical Z-planes in CTRL, SGEF KD, and Rescue WT MDCK cells stained for endogenous ZO-1 and mNeon-SGEF (green). The bottom panels show a zoomed image of the selected regions (dotted yellow line). Scale bars, top panel: 20 µm; bottom panels: 10 µm. **(B–D)** Quantification of zigzag index, apical cell area, and axial ratio in CTRL, SGEF KD, and Rescue WT cells. Two fields from two independent experiments were used for quantification. (*n* = at least 75 cells for zigzag index, *n* = 100 for area and *n* = 150 for axial ratio). Error bars represent min to max values. **(E)** TEER of CTRL, SGEF KD, and Rescue WT cells is plotted. Data represent the average of three experiments performed in duplicates. CTRL was normalized to 1, and data were plotted relative to CTRL. Error bars represent SEM. *, P < 0.05; **, P < 0.005; ***, P < 0.0005; ****, P < 0.00005; *ns*, nonsignificant using the Mann–Whitney *U* test (B–D) or Student's *t* test (two-tailed, unpaired; E).

with the inhibitors for 16 h, which in some cases can elicit compensatory effects (Choi et al., 2016). Nevertheless, this suggests that the increase in contractility observed in response to SGEF depletion is mediated by the ROCK/myosin II pathway.

The similarities between the SGEF KD and ZO-1/2 KD phenotypes suggest that SGEF and ZO-1 may be operating within the same pathway. Interestingly, analysis of ZO-1 fluorescence intensity at TJs showed that it decreased significantly when SGEF was silenced and was rescued by SGEF reexpression (Fig. 7 C). A similar result was obtained when we analyzed the levels of ZO-1 by WB (Fig. 7 D). These results place SGEF upstream of ZO-1, regulating its expression levels. We also analyzed the expression and localization of afadin, an adapter protein that interacts with cytoskeleton and junctional proteins (Takai and Nakanishi, 2003). In ZO 1/2 KD cells, afadin is recruited to AJs and is especially enriched at TCJ (Choi et al., 2016). In SGEF KD cells, both the expression levels of afadin and its localization at AJs are reduced (Fig. 7, D and E). However, the reduction observed in afadin targeting to AJ is not uniformly distributed along AJ, as afadin signal intensity remained high at TCJ, but was dramatically reduced at BCJ (Fig. 7 E). Quantification of the ratio of intensity at the TCJ versus BCJ showed a significant increase when SGEF is KD, confirming the enrichment at the TCJ (Fig. 7 F). Both the expression and localization of afadin were rescued to normal levels upon reexpression of mNeon-SGEF WT (Fig. 7, D–F). These results suggest that silencing SGEF and ZO-1/2 elicits a similar but not identical response, redistributing afadin to TCJ in response to an increase in junctional actomyosin tension (Choi et al., 2016). Taken together, our results suggest that SGEF might function in a similar pathway as ZO 1/2 and afadin, regulating AJC architecture and function by regulating actomyosin-mediated junctional tension.

SGEF overexpression promotes apical constriction in *Xenopus* embryos

SGEF localizes to apical junctions when expressed in gastrula-stage *Xenopus* embryos (Fig. 4). We noticed that when SGEF was expressed at low levels, there were no major differences in the general appearance of the cell–cell junctions. However, in cells expressing higher levels, the apical surface area was significantly smaller. To confirm this gain of function phenotype, we overexpressed 3xGFP-SGEF WT at a high level in *Xenopus* embryos and analyzed the effects on TJ using mRFP-ZO-1 as a marker. First, we found that SGEF overexpressing (OE) cells were frequently apically constricted (yellow arrows in Fig. 8 A). Live imaging analysis showed that 3xGFP-SGEF–expressing cells

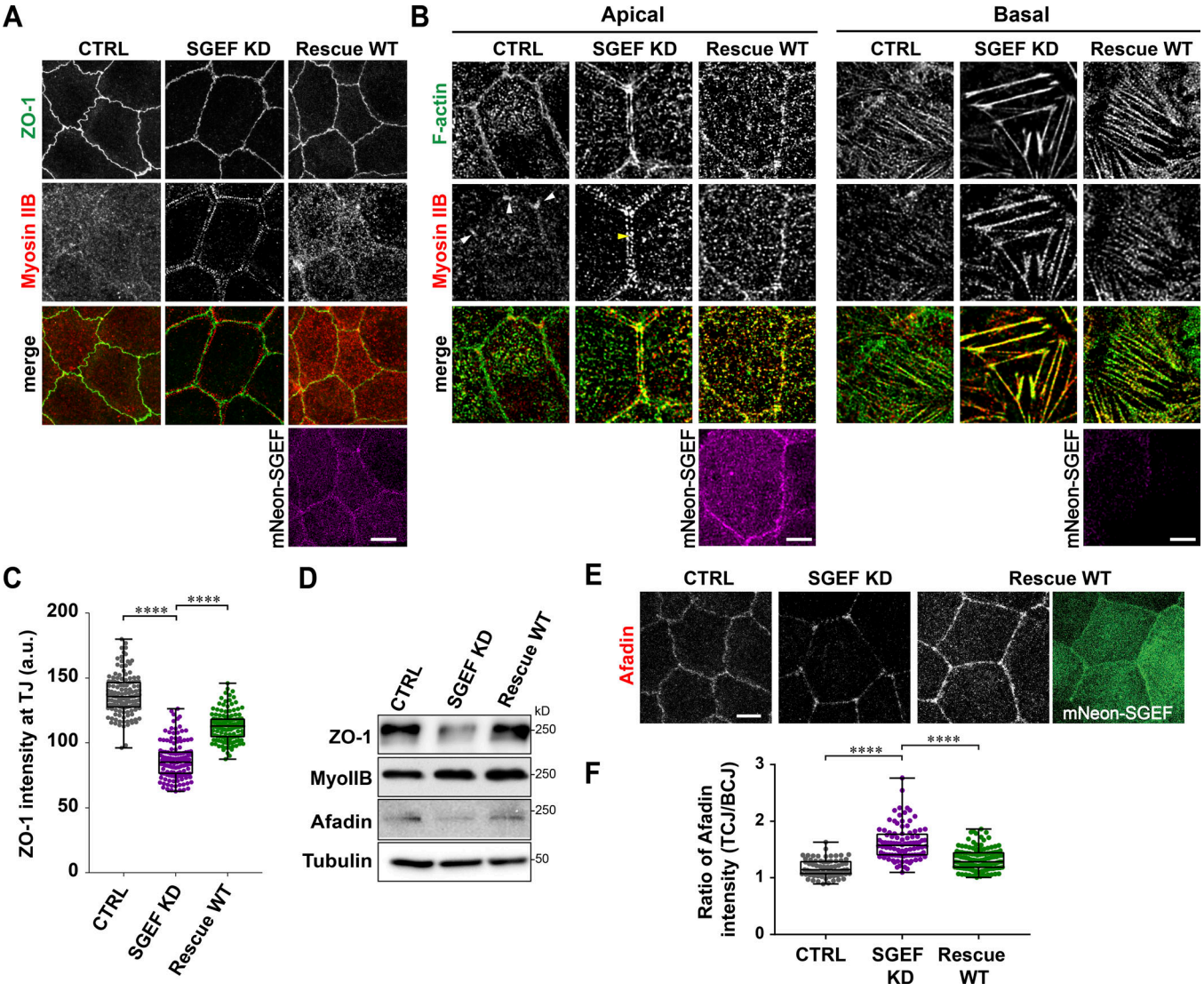

Figure 7. **SGEF KD stimulates actomyosin contractility. (A)** Confocal images showing maximum projection of apical Z-sections in CTRL, SGEF KD, and Rescue WT MDCK cells stained for endogenous ZO-1 (green), myosin IIB (red), and mNeon-SGEF (magenta, in Rescue). mNeon signal is shown in magenta in Rescue panel to maintain color consistency. Scale bar, 5 µm. **(B)** Confocal images showing CTRL, SGEF KD, and Rescue WT MDCK cells stained for endogenous F-actin using phalloidin (green) and myosin IIB (red). Left panel: Maximum projection of apical Z-planes; right panel: maximum projection of basal Z-planes. Images were processed using the HyVolution deconvolution package (see Materials and methods). Scale bars, 0.5 µm. **(C)** Quantification of intensities of ZO-1 at junctions measured using a rectangle of 2 × 3 µm placed along BCJs. At least two fields from two independent experiments were used for quantification (≥100 junctions). Error bars represent SEM. ****, $P < 0.00005$; *ns*, nonsignificant using the Mann–Whitney *U* test. **(D)** Total cell lysates from confluent CTRL, SGEF KD, and Rescue WT MDCK cells were immunoblotted with ZO-1, myosin IIB, and afadin antibodies. Tubulin was used as a loading control. **(E)** Maximum projection of confocal images showing the localization of endogenous afadin in CTRL, SGEF KD, and Rescue WT cells. Scale bar, 5 µm. **(F)** Quantification of the ratio of TCJ over BCJ intensity of afadin was measured as described in Materials and methods. At least three fields from two independent experiments were used for quantification (≥200 junctions). Error bars represent SEM. ****, $P < 0.00005$; *ns*, nonsignificant using the Mann–Whitney *U* test.

constrict over time, whereas CTRL cells remain quite stable over that time frame (Fig. 8 B and Videos 1 and 2). Live imaging analysis of mRFP-ZO-1 dynamics showed that in CTRL cells, ZO-1 appears quite stable over time, whereas in SGEF OE cells, ZO-1 was very dynamic at junctions (Fig. 8, B and C). Quantification confirmed that SGEF OE cells had smaller apical areas on average due to apical constriction when compared with CTRL cells (Fig. 8 D).

Apical actomyosin activity is known to drive constriction and other morphogenetic processes during development (Röper, 2013; Munjal and Lecuit, 2014). As SGEF OE cells were apically constricted, we analyzed F-actin accumulation in *Xenopus* gastrula-stage epithelial cells. In fixed phalloidin-stained samples, F-actin was significantly increased at both the junctional and medial-apical regions in SGEF OE cells (Fig. 8, E, E′, and E′′). We also analyzed the effects of overexpressing SGEF on the local accumulation of F-actin and myosin II in live *Xenopus* embryos by coexpressing an F-actin probe (Lifeact-mRFP) and a myosin II intrabody (SF9-mNeon). Compared with CTRL, SGEF overexpression resulted in increased and reorganized junctional and

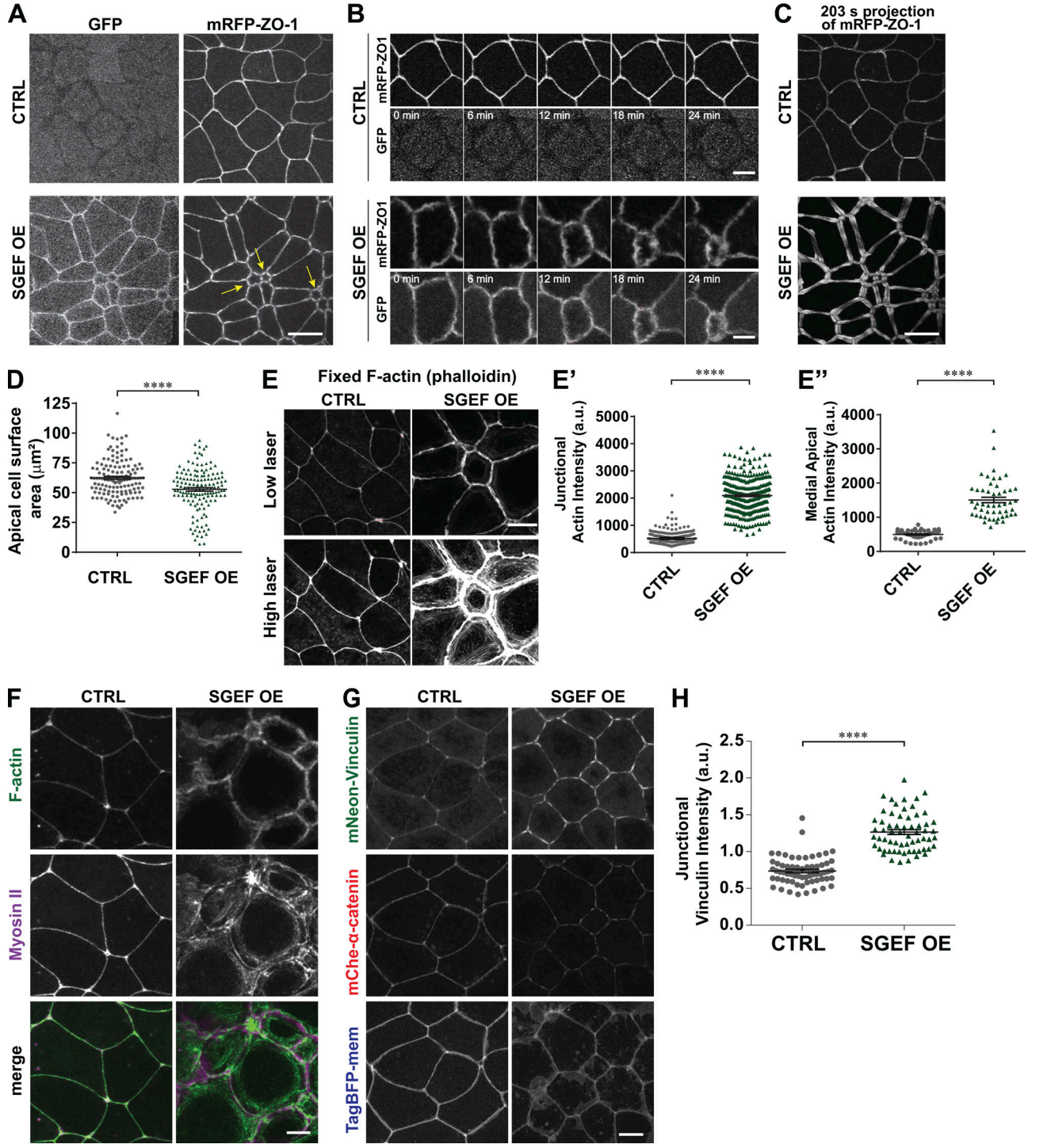

Figure 8. **SGEF regulates apical constriction in epithelial cells. (A)** Gastrula-stage *Xenopus* embryos expressing mRFP-ZO-1 (TJ marker) with 3xGFP-SGEF overexpressed (OE) at high levels (bottom). Yellow arrows point to apically constricted cells. Scale bar, 20 µm. **(B)** Time lapse of CTRL and 3xGFP-SGEF overexpression of a single cell over a period of 24 min. Note that the SGEF OE cell constricts apically whereas CTRL cell retains the same apical area. Scale bars, 10 µm. **(C)** Time projection of ZO-1 signal over a 203-s interval shows that junctions in SGEF OE cells are more dynamic than in CTRLs. Scale bar, 20 µm. **(D)** Graph showing the average apical surface area of SGEF OE cells is significantly smaller than CTRL cells, and some SGEF OE cells exhibit severe apical constriction. CTRL, *n* = 132 cells, three embryos, two experiments; SGEF OE, *n* = 147 cells, three embryos, two experiments. **(E)** CTRL and SGEF OE gastrula-stage *Xenopus* embryos were fixed and stained with Alexa Fluor 568–phalloidin to reveal F-actin. Images in the top row were taken with lower laser power optimized for viewing cell–cell junctions, and images in the bottom row were taken with higher laser power optimized for viewing medial-apical actin. Scale bar, 10 µm. **(E′)** F-actin intensity at BCJ was quantified from fixed phalloidin stained embryos. *n* = control: 288 junctions, 11 embryos, three experiments; SGEF OE: 304 junctions, 13 embryos, two experiments. **(E′′)** Medial-apical F-actin intensity was quantified from fixed phalloidin stained embryos. *n* = control: 50 cells, seven embryos, three experiments; SGEF OE: 50 cells, eight embryos, three experiments. **(F)** CTRL and SGEF OE embryos expressing an F-actin probe (Lifeact-mRFP, magenta in merge) and a myosin II intrabody (SF9-mNeon, green in merge) were live imaged by confocal microscopy. The control image shown is from a

control region of a mosaic SGEF OE embryo. Scale bar, 10 µm. **(G)** CTRL and SGEF OE embryos coexpressing mNeon-Vinculin, mCherry-α-catenin, and BFP-membrane. Scale bar, 10 µm. **(H)** Graph comparing junctional intensities of vinculin (normalized to membrane probe intensity) in CTRL and SGEF OE embryos. *n* = control: 63 junctions, eight embryos, three experiments; SGEF OE: control: 63 junctions, eight embryos, three experiments. Confocal images in A, B, and E–G are brightest point of apical sections. All graphs show mean ± SEM. ****, P < 0.00005 using the Mann–Whitney *U* test.

medial-apical F-actin and myosin II; F-actin was broader at cell–cell junctions, whereas myosin II was reorganized into a strong band interior to cell–cell junctions (Fig. 8 F).

α-Catenin links the AJ to the actin cytoskeleton (Buckley et al., 2014). When α-catenin senses increased junctional tension generated by the actomyosin cytoskeleton, it undergoes a conformational change, recruiting vinculin and thus strengthening the AJ's connection to F-actin (Yonemura et al., 2010). Therefore, the recruitment of fluorescently tagged vinculin to junctions can be used as a readout for increased junctional tension (Hara et al., 2016; Higashi et al., 2016). In control *Xenopus* embryos, mNeon-Vinculin was weakly recruited to cell–cell junctions, whereas in SGEF OE embryos, mNeon-Vinculin was strongly recruited to junctions and was particularly increased near TCJs (Fig. 8, G and H). These results indicate that in developing *Xenopus* embryos, SGEF plays a role in the regulation of apical actomyosin constriction.

SGEF's nucleotide exchange activity is required for junctional maintenance whereas its scaffolding activity is required for apical contractility

SGEF activates RhoG, a Rho GTPase related to Rac that plays a role in a variety of cellular processes, including cell migration, invasion, macropinocytosis, and neurite outgrowth (Katoh et al., 2000, 2006; Ellerbroek et al., 2004; van Buul et al., 2007; Jackson et al., 2015; Goicoechea et al., 2017; Valdivia et al., 2017). Our results suggest that SGEF is playing a role in both the formation and maintenance of cell–cell junctions, as well as in the regulation of apical contractility. How is SGEF orchestrating these processes? One possibility is that SGEF is recruited to junctions in order to activate RhoG locally. Alternatively, SGEF could function as a scaffold to mediate the formation of the Scribble/SGEF/Dlg1 ternary complex. To explore these possibilities, we first analyzed the effect of silencing SGEF on the activity levels of RhoG in MDCK cells. Using a RhoG activity pulldown assay (van Buul et al., 2007), we found that the activity of RhoG was significantly reduced when SGEF expression was silenced (Fig. 9, A and B). Active RhoG levels returned to normal when SGEF expression was rescued with mNeon-SGEF WT (Rescue WT), but not when rescued with a catalytic dead (CD) mutant of SGEF (R446A, N621A; Rescue CD; Ellerbroek et al., 2004; Fig. 9, A and B). These results indicate that modulating the expression levels of SGEF in MDCK cells has a significant effect on the endogenous levels of active RhoG.

To explore the contributions of the catalytic and scaffolding activities of SGEF, we generated stable cell lines expressing three different SGEF mutants in the background of SGEF KD cells and tested their ability to rescue the key phenotypes described in Figs. 5, 6, and 7 for SGEF KD cells (i.e., the strong reduction in E-cadherin, straight TJs, and increased actomyosin contractility). First, SGEF 1–227 is a construct that binds to Scribble but not to Dlg1 (see Fig. 2), so it cannot form a ternary complex (no scaffolding activity) and has no exchange activity. Second, SGEF 1–400 is a construct that expresses only the minimum region required to bind Scribble and Dlg1, so it has scaffolding activity (can form a ternary complex; see Fig. 3), but has no catalytic activity. Finally, SGEF CD is a CD full-length SGEF that contains the binding sites for both Scribble and Dlg1 (scaffolding), as well as all the other domains in SGEF. Interestingly, none of the three constructs tested were able to rescue the reduction in E-cadherin protein level observed in SGEF KD cells (Fig. 9, C, D, and H). This suggested that the catalytic activity of SGEF, and thus RhoG activation, is required for the regulation of E-cadherin expression. Similar results were observed for β-catenin, which loses its tight localization to junctions in SGEF KD cells and could not be rescued by any of the three constructs tested (Fig. 9 E). As none of the SGEF mutants tested (1–227, 1–400, and CD) rescued the reduction in E-cadherin or the disorganized β-catenin localization at AJs, we hypothesized that these mutants would not be able to rescue the reduced height phenotype observed in SGEF KD cells either. As expected, none of the three SGEF mutants rescued the cell height defect. The average height in cells expressing each of the three SGEF mutants was within the same range of the height measured in SGEF KD cells, approximately two times shorter than that of CTRL cells (CTRL: 5.95 ± 0.18 µm, SGEF KD: 2.5 ± 0.02 µm, Rescue 1–227: 2.99 ± 0.065 µm, Rescue 1–400: 2.57 ± 0.049 µm, and Rescue CD: 3.009 ± 0.064 µm; Fig. 9, F and I).

Interestingly, the mutants that can form a ternary complex but have no catalytic activity (SGEF 1–400 and SGEF CD) were able to rescue the straight TJ phenotype observed in SGEF KD cells (Fig. 9, G and J). Quantification of the linearity of the TJs showed that, although not completely rescued to the levels observed in CTRL cells, the zigzag index increased significantly in both Rescue 1–400 and Rescue CD cells when compared with SGEF KD (Fig. 9 J). Both mutants were also able to rescue the increase in contractility observed in SGEF KD cells, reverting the formation of the apical actomyosin array to a more diffuse myosin II staining around junctions like the pattern found in CTRL cells (Fig. 9 G).

Overall, our results demonstrate that the regulation of E-cadherin–mediated AJ formation and maintenance requires the exchange activity of SGEF, whereas the ability of SGEF to function as a scaffold by forming the Scribble/SGEF/Dlg1 ternary complex is important for regulating junctional actomyosin contractility and normal junctional architecture.

SGEF KD does not affect polarity but impairs lumen formation in MDCK 3D cysts

When MDCK cells are embedded in a 3D ECM such as matrigel or collagen, they form a polarized spherical cyst with a fluid-filled hollow lumen surrounded by a monolayer of polarized cells

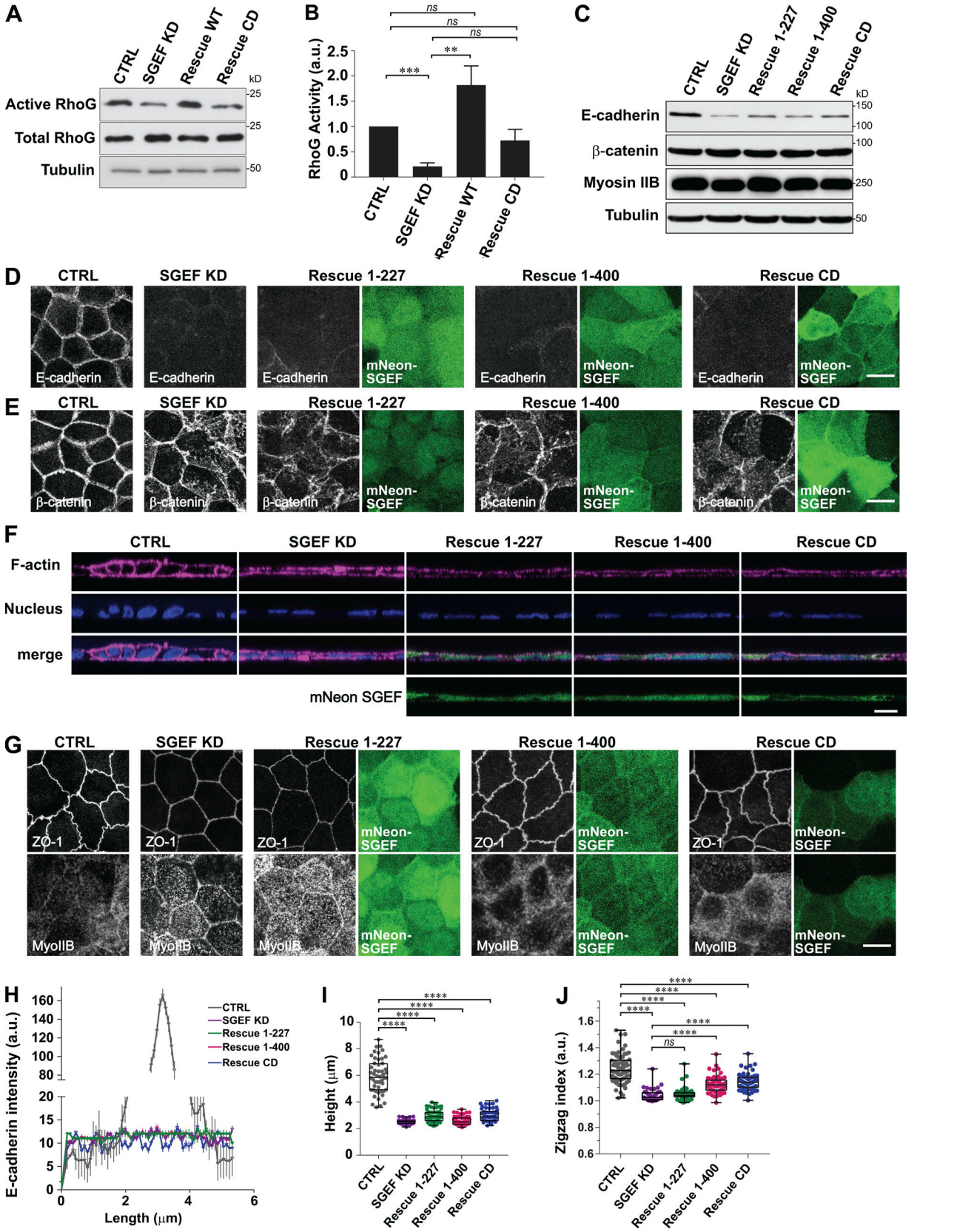

Figure 9. **The guanine nucleotide exchange activity of SGEF is required for junctional maintenance, whereas scaffolding activity of SGEF is required for apical contractility. (A)** Active RhoG was precipitated from total lysates of CTRL, SGEF KD, Rescue mNeon-SGEF WT, and Rescue CD mNeon-SGEF using GST–ELMO and immunoblotted with anti-RhoG antibodies. **(B)** For quantification, active RhoG levels were normalized to total RhoG levels. Data are mean ± SEM of three independent experiments. **, P < 0.005; *ns*, nonsignificant using Student's *t* test (two-tailed, unpaired). **(C)** Lysates from CTRL, SGEF KD, and

SGEF KD cells rescued with mNeon-SGEF 1–227, mNeon-SGEF 1–400, or mNeon-SGEF CD were probed for E-cadherin, β-catenin, ZO-1, and myosin IIB antibodies. Tubulin was used as a loading control. **(D and E)** Confluent MDCK CTRL, SGEF KD, and SGEF KD cells rescued with mNeon-SGEF 1–227, mNeon-SGEF 1–400, or mNeon-SGEF CD were stained for endogenous E-cadherin, β-catenin, and mNeon-SGEF (green). Confocal images are maximum projections of apical Z-planes. Scale bar, 5 µm. **(F)** XZ view of MDCK cells from CTRL, SGEF KD, and SGEF KD cells rescued with mNeon-SGEF 1–227, mNeon-SGEF 1–400, or mNeon-SGEF CD stained for F-actin (magenta), nucleus (Hoechst), and mNeon-SGEF (green). Scale bar, 10 µm. **(G)** Confluent MDCK CTRL, SGEF KD, and SGEF KD cells rescued with m-Neon-SGEF 1-227, mNeon-SGEF 1-400, or mNeon-SGEF CD were steined for endogenous ZO-1, myosin IIB, and mNeoen-SGEF (green). Confocal images are maximum projections of apical Z-planes. Scale bar, 5 µm. **(H)** Linescan (6-µm line drawn perpendicular to center of junctions) of IF images in D. At least two fields from two independent experiments (≥150 junctions) were used for quantification. The intensity profiles from were manually centered around the highest peak for each condition. **(I)** Quantification of height in CTRL, SGEF KD, and SGEF KD cells rescued with mNeon-SGEF 1–227, mNeon-SGEF 1–400, or mNeon-SGEF CD cells. $n = 50$ cells for each condition. Error bars represent min to max values with all points. Error bars represent SEM. ****, $P < 0.00005$, using the Mann–Whitney U test. **(J)** Quantification of zigzag index of CTRL, SGEF KD, and SGEF KD cells rescued with mNeon-SGEF 1–227, mNeon-SGEF 1–400, or mNeon-SGEF CD. At least two fields from two independent experiments (≥200 junctions) were used for quantification. ****, $P < 0.00005$; *ns*, nonsignificant using Student's t test (two-tailed, unpaired).

(O'Brien et al., 2002). The organization of these cysts resembles that of epithelia in vivo, and thus, cyst development provides a model system for the formation of epithelial morphogenesis in vitro. We used this system to test the potential role of SGEF in the establishment of apicobasal polarity and cyst morphogenesis. First, we determined whether SGEF was required for the establishment of apicobasal polarity in 2D MDCK cultures, where cells form a columnar monolayer with a well-defined apical and basal membrane. Our results showed that in SGEF KD cells, the apical membrane marker gp135/podocalyxin (Ojakian and Schwimmer, 1988) targeted efficiently to the apical surface (Fig. 10 A). These results suggested that even though silencing SGEF induced dramatic changes in TJ and AJ architecture (Fig. 5 and 6) and cell height (Fig. 5), it did not affect apicobasal polarity. We then generated cysts by embedding CTRL, SGEF KD, and Rescue WT cells in matrigel and allowing them to grow for 4 d. We stained the cysts with different markers, including β-catenin and E-cadherin (AJ), gp135 (polarity), and F-actin. Our results showed that in CTRL cells, most cysts had a single open lumen that was properly polarized (65%), with β-catenin and E-cadherin decorating the lateral junctions, and gp135 and F-actin concentrated at the apical surface (toward the luminal surface inside of the cyst; Fig. 10, B–D). The rest of the CTRL cysts contained more than one lumen (multiple), which were all open (35%; Fig. 10, B–D). In contrast, 77% of the SGEF KD cysts were severely disorganized with no obvious central lumen. Instead of a single open lumen, SGEF KD cysts displayed multiple gp135-positive patches, the majority of which were closed, or, when open, had a very small lumen (Fig. 10, B and D). This suggested that despite the severity of the SGEF KD phenotype, the establishment of apicobasal polarity was not affected, as gp135 was properly targeted to the apical membrane (Fig. 10 B). β-Catenin still localized to lateral membranes in SGEF KD cysts (Fig. 10 B), but E-cadherin was significantly down-regulated (Fig. 10 C), which was consistent with our observations in 2D cultures. Reexpression of mNeon-SGEF WT (Rescue WT) restored the normal phenotype. The majority of the Rescue WT cysts had open lumens (75%), either single (35%) or multiple (40%; Fig. 10, B–D), and E-cadherin expression was also restored to normal levels (Fig. 10 C). These results indicate that, even though SGEF does not play a major role in the establishment of polarity, it regulates both the ability of cysts to form an open lumen and the number of lumens formed in each cyst.

To explore the contribution of the catalytic and scaffolding activities of SGEF during cyst formation, we also generated cysts using the stable Rescue CD cells described in Fig. 9, which express a full-length CD mutant of SGEF in SGEF KD cells. Our results showed that, in agreement with the results obtained in 2D monolayers, the expression of E-cadherin was not rescued in Rescue CD cysts, confirming the requirement of the exchange activity for the regulation of E-cadherin levels (Fig. 10 C). In addition, expression of SGEF CD did not rescue the ability of the cysts to form a single central lumen (Fig. 10 C and Fig. S5). Quantification showed that the number of cysts that had a single lumen decreased from 65% in CTRL cells to 13% in SGEF KD cells. Rescue WT increased the number of single lumens to 36%, whereas in Rescue CD cysts, only 14% had a single lumen (Fig. 10 D, red and dark green bars). To our surprise, the scaffolding activity of SGEF appeared to be required during lumen opening, as SGEF CD expression significantly restored the number of cysts that formed open lumens (Fig. 10 C and Fig. S5). Quantification demonstrated that the number of cysts with an open lumen decreased from 100% in CTRL cells to 23% in SGEF KD cells. Reexpression of SGEF WT and SGEF CD restored the number of cysts with open lumens to 77% and 59%, respectively (Fig. 10 D, red and orange bars). Overall, these results suggest that SGEF plays a role during lumen formation in 3D cysts. The catalytic activity of SGEF is important for formation of a cyst with a single lumen, which may depend on the regulation of E-cadherin expression (see Discussion). The scaffolding activity, on the other hand, is required for the formation of a fluid-filled open lumen.

Discussion

The formation of a polarized epithelium requires the coordinated action of three highly conserved protein complexes: PAR, Crumbs, and Scribble (Bilder et al., 2003). These polarity protein complexes act as scaffolds recruiting other proteins in response to both intracellular and extracellular cues, which ultimately result in the reorganization of the cytoskeleton and vesicular trafficking that leads to the establishment of cellular asymmetry (Rodriguez-Boulan and Macara, 2014).

The Scribble complex was initially identified in *Drosophila* as a critical regulator of epithelial polarity (Gateff and Schneiderman, 1974; Mechler et al., 1985; Woods and Bryant, 1991; Bilder and

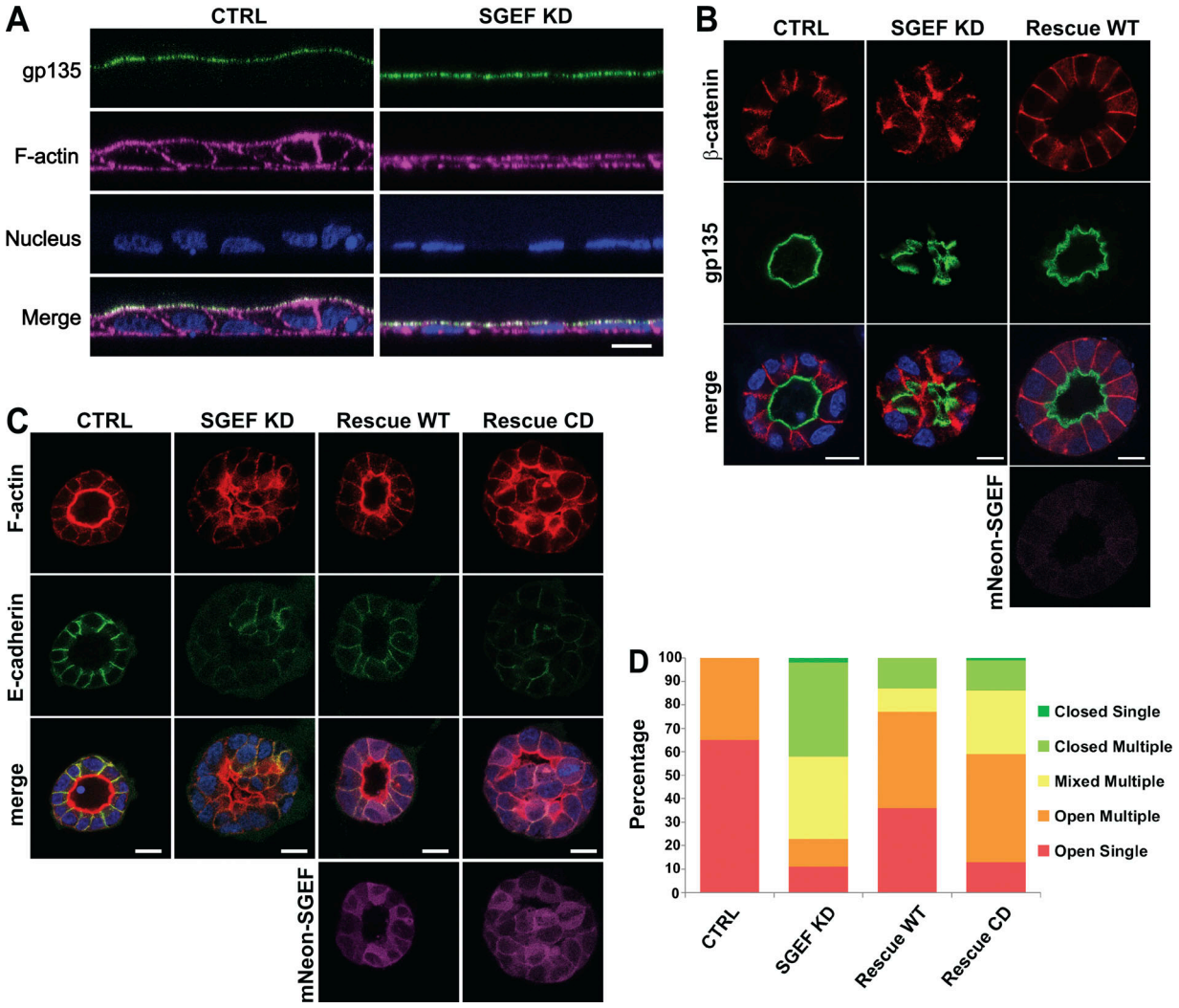

Figure 10. **SGEF does not affect polarity but regulates lumen formation in 3D MDCK cysts. (A)** IF of MDCK CTRL and SGEF KD cells using gp135 (green), actin (magenta), and nucleus (Hoechst). Scale bar, 10 µm. **(B and C)** MDCK CTRL, SGEF KD, and Rescue WT cells were plated on matrigel to form 3D cysts. Cysts were fixed and stained for β-catenin (red), gp135 (green), and nuclei (blue) in B and E-cadherin (green), phalloidin (red), and nuclei (blue) in C. For detailed protocol of growing and staining cyst, see Materials and methods. Scale bars, 5 µm. **(D)** Cysts from CTRL, SGEF KD, Rescue WT, and Rescue CD were classified based on the number of cysts (single or multiple) and the phenotype of the lumen (open or closed). Three independent experiments were counted for each condition (≥200 cysts/condition). Images in B and C are single Z-sections corresponding to the center of the cyst.

Perrimon, 2000) and was later shown to be involved in the regulation of other cellular processes, including cell–cell adhesion, asymmetric cell division, vesicular trafficking, cell migration, and planar-cell polarity (Elsum et al., 2012). The canonical Scribble complex is comprised of three proteins, Scribble, Dlg, and Lgl, which are thought to function in a common pathway (Elsum et al., 2012). However, the molecular mechanisms that regulate their physical interactions and functions are poorly characterized.

In this study, we show that SGEF, a RhoG-specific GEF, forms a ternary complex with two of the members of the Scribble polarity complex, Scribble and Dlg1. The formation of this ternary complex positions SGEF at cell–cell junctions, where it regulates the formation and maintenance of AJs, as well as actomyosin contractility and barrier function at TJs. SGEF does not appear to affect apicobasal polarity in 3D cysts, but it plays a role during lumen formation.

Our results provide a detailed map of the interaction between these three proteins. SGEF interacts with the GUK domain of Dlg1 through an unstructured 50-aa motif and with Scribble PDZ1 domain through a novel iPBM. Although PBMs are typically located at the extreme C terminus of a protein (Songyang et al., 1997), a small number of iPBMs have been identified (Brenman and Bredt, 1997; Hillier et al., 1999; Wong et al., 2003; London et al., 2004; Penkert et al., 2004; Mu et al., 2014). In contrast to the C-terminal PBMs, a consensus motif for the iPBMs identified so far has not been defined. The structure of the Scribble PDZ1–SGEF interaction is also very different, and the two proteins make much more extensive contacts compared with the two previously published PDZ/iPBM structures (Hillier et al., 1999; Penkert et al., 2004). Interestingly, SGEF encodes a second PBM at its C terminus (type I). Our results show that it does not interact with any of the seven PDZ domains encoded by

Scribble and Dlg1, suggesting that it may function to recruit other interacting partners to the Scribble complex.

Our results show that the interaction is mediated by the GUK domain of Dlg1 and a stretch of 50 aa in the N terminus of SGEF. However, a previous report had described the interaction between SGEF and Dlg1 and mapped the interaction to SGEF's PBM and Dlg1's PDZ domains 1–2 (Krishna Subbaiah et al., 2012). Interestingly, the initial report also showed that SGEF and Dlg1 were able to interact when the PBM in SGEF and PDZ domains in Dlg1 were deleted. Moreover, the GUK domain of Dlg1 was shown to interact with a mutant of SGEF in which the SH3 and PBM were deleted. It is possible that the PBM–PDZ interaction observed by Krishna Subbaiah et al. (2012) resulted from the way these assays were performed, i.e., using a high concentration of GST-tagged proteins expressed in bacteria. The specificity of a PBM–PDZ interaction in vitro only demonstrates its potential binding capability, but it does not necessarily mean that interaction should exist in vivo. Here, the C terminus of SGEF has the potential to bind Dlg1 in vitro, but our data indicate it does not bind in vivo.

SGEF belongs to a small subfamily of six related GEFs called ephexins (Rossman et al., 2005), but the Scribble and Dlg1 binding sites are only found in SGEF. Both binding interfaces are located at SGEF's N terminus and are highly conserved among vertebrates. SGEF orthologues do not seem to be present in *Drosophila* or other invertebrates. The closest homologue in *Drosophila* is ephexin, which lacks the N-terminal Scribble/Dlg1 binding region and is more closely related to ephexin 4 in humans.

Interestingly, the formation of a ternary complex including Scribble and Dlg appeared at least one more time during evolution. In *Drosophila*, a protein called GUK-holder (GUKH) also forms a ternary complex with Dlg1 and Scribble (Mathew et al., 2002). Like SGEF, GUKH binds to the GUK domain of Dlg1 and to PDZ1 in Scribble, although through a C-terminal PBM (Mathew et al., 2002; Caria et al., 2018). In contrast to SGEF, GUKH functions exclusively as a scaffold and has no known enzymatic activity. GUKH plays a role in the development of *Drosophila* epithelial tissues, and silencing GUKH enhances the defects caused by Scribble or Dlg depletion in eyes and wings (Caria et al., 2018). Two GUKH orthologues have been identified in humans, Nance-Horan syndrome (NHS) and NHSL1 (Katoh and Katoh, 2004). NHS proteins localize to cell junctions and also associate with Scribble and the Dlg family member PSD95 (Dlg4). However, the ability of NHS to mediate the formation of a ternary complex has not been demonstrated (Sharma et al., 2006; Walsh et al., 2011). It is tempting to speculate that the function of *Drosophila* GUKH is conserved in humans in the NHS family, and SGEF regulates a different function that appeared later during vertebrate evolution. It also raises the possibility that in vertebrates, different ternary complexes could coexist in the same cell, and could possibly regulate different processes.

In mammalian cells, both Scribble and Dlg1 are targeted to cell–cell junctions, where they are distributed throughout the lateral membrane and colocalize with both AJ and TJ markers (Dow et al., 2003; Laprise et al., 2004; Navarro et al., 2005; Ivanov et al., 2010). Our results show that SGEF targets to cell–cell junctions in a Scribble-dependent manner, where it also colocalizes with AJ and TJ markers. Targeting SGEF to junctions is important for Dlg1 recruitment and to a lesser extent may also help recruit or maintain Scribble at the right location. When SGEF expression is silenced, the most striking phenotype is an almost complete loss of E-cadherin protein expression, which is accompanied by disorganized AJs, a collapse of the lateral membrane, and a threefold decrease in cell height. Silencing Scribble or Dlg1 in mammalian cells also affects AJ architecture in a similar fashion, although the effects are typically milder and are not associated with significant E-cadherin down-regulation (Laprise et al., 2004; Qin et al., 2005; Hendrick et al., 2016). Surprisingly, neither β-catenin nor p120-catenin is down-regulated upon SGEF KD, where the E-cadherin expression level is strongly reduced, and cells can still form a monolayer. Moreover, β-catenin and α-catenin are still localized to AJ when E-cadherin expression is silenced to almost undetectable levels (Capaldo and Macara, 2007). This could be a result of compensation by other cadherins, which are up-regulated in the absence of E-cadherin (Tinkle et al., 2004; Tunggal et al., 2005). We found that cadherin-6, which is expressed at high levels in MDCK cells (Stewart et al., 2000), is up-regulated in SGEF KD cells. This may contribute to maintaining the monolayer integrity in the absence of E-cadherin, although it is not sufficient to restore normal AJ architecture. As in E-cadherin KD cells (Capaldo and Macara, 2007), SGEF KD affects primarily the establishment of junctions but not the maintenance of already established junctions. Interestingly, down-regulation of E-cadherin expression is a hallmark of epithelial-to-mesenchymal transition (EMT; Kalluri and Weinberg, 2009). Despite a drastic decrease in E-cadherin levels, we see no phenotypic indication of EMT in SGEF KD cells. This is not completely unexpected, as studies in normal cells have shown that E-cadherin loss is not always sufficient to induce EMT (Chen et al., 2014). It is possible that the partial compensation by cadherin-6 and/or other cadherins plays a role in preventing EMT.

Besides its role in regulating AJ structure, SGEF also regulates the structure and function of TJs. In SGEF KD MDCK cells, TJs lose their typical curvilinear morphology and become very straight, with cells adopting an isometric polygonal shape. In addition, a highly contractile junctional actomyosin array accumulates at junctions in SGEF KD cells, which increases tension at the AJC. A strikingly similar phenotype has been described in ZO-1 KD/KO (Van Itallie et al., 2009; Tokuda et al., 2014) and ZO-1/ZO-2 double KD in MDCK cells (Fanning et al., 2012; Choi et al., 2016), as well as during Shroom overexpression (Hildebrand, 2005). Both ZO-1/ZO-2 and Shroom function upstream of ROCK (Hildebrand, 2005; Choi et al., 2016), suggesting that SGEF may also operate directly or indirectly in a pathway that regulates ROCK recruitment and/or activation.

Notably, silencing SGEF has a much broader and more severe impact on both AJs and TJs than in the aforementioned studies (Hildebrand, 2005; Fanning et al., 2012; Choi et al., 2016), with a strong reduction in E-cadherin protein level, disorganized AJs, reduced cell height, and disrupted barrier function, which have not been observed when Scribble or Dlg1 was silenced (Laprise et al., 2004; Qin et al., 2005; Choi et al., 2016; Hendrick et al.,

2016), or upon Shroom overexpression (Hildebrand, 2005). ZO-1 KO/ZO-2 KD epithelial cells (Eph4) are unable to form TJ strands and exhibit significant increase in paracellular permeability of large solutes and a decrease in TEER (Umeda et al., 2006). In MDCKs, ZO-1/ZO-2 double KD MDCK cells exhibit a similar phenotype with increased paracellular permeability of large solutes but no change in TEER (Fanning et al., 2012). This suggests that SGEF may also function in other pathways in parallel to those in which Scribble, Dlg1, and ZO-1 are involved. Alternatively, it can be attributed to differences in the efficiency of KD, or to the use of different cell lines in the previous studies that could result in milder phenotypes.

SGEF has been shown to direct actin cytoskeleton remodeling at both the dorsal and ventral surface of the cells, but never before at cell–cell junctions (Ellerbroek et al., 2004; Patel and Galán, 2006; van Buul et al., 2007; Goicoechea et al., 2017). Our study delineates two very well-defined roles for SGEF, which can be classified according to their dependence on SGEF's nucleotide exchange activity. The regulation of E-cadherin stability and proper AJ architecture requires the nucleotide exchange activity of SGEF, suggesting it is mediated by RhoG. On the other hand, SGEF-mediated regulation of junctional contractility is independent of its exchange activity, and only requires the ability of SGEF to form a ternary complex with Scribble and Dlg1. The molecular mechanisms that control these two processes are not known. A potential candidate connecting RhoG activity and AJ formation is the RhoG effector ELMO2. ELMO2 is expressed in MDCKs and has been shown to play a role, together with the Rac1 GEF DOCK1, in recruiting E-cadherin to junctions (Toret et al., 2014). However, silencing either ELMO2 or DOCK1 only delays junction formation and has no effect on E-cadherin expression levels (Toret et al., 2014), which suggests that SGEF and RhoG may function through a yet to be characterized pathway. Regarding the role of the Scribble/SGEF/Dlg1 ternary complex in the regulation of junctional contractility and TJ morphology, virtually nothing is known. Scribble has been shown to interact with ZO-1/ZO-2, suggesting the ternary complex may be physically linked to TJs (Métais et al., 2005; Ivanov et al., 2010). Our future efforts are aimed to characterize the downstream signaling pathways that connect SGEF with AJ and TJ function.

Overexpression of SGEF in *Xenopus* epithelial cells induces a different contractility phenotype, with a dramatic accumulation of F-actin and myosin II at the apical belt, which leads to apical constriction and reduced apical cell area. At the apical surface, actin polymerization and actomyosin contractility are regulated by the coordinated actions of several GTPases, including RhoA, Rac1, and Cdc42. This requires a tight control of the spatial and temporal activation pattern of each of the GTPases involved. The molecular mechanisms controlling these processes are still not well characterized, but several RhoGEFs and RhoGAPs are identified to modulate this process (Aijaz et al., 2005; Sousa et al., 2005; Terry et al., 2011; Holeiter et al., 2012; Nishimura et al., 2012; Ratheesh et al., 2012; Tripathi et al., 2012; Ngok and Anastasiadis, 2013; Zebda et al., 2013; Breznau et al., 2015). Silencing the expression of these GEFs and GAPs alters junction integrity or interferes with contractility, suggesting that multiple GEFs and GAPs regulate different functions at cell junctions (Ratheesh et al., 2013; Ngok et al., 2014). Interestingly, the RhoA-GAP DLC3 and the Rac1-GEF β-PIX interact with Scribble to locally control RhoA and Rac1 activity along the lateral membrane of epithelial cells (Audebert et al., 2004; Hendrick et al., 2016). It is possible that SGEF's interaction with Scribble and Dlg1 also contributes to the regulation of the balance of the different GTPases that function at cell junctions and control contractility. This could be mediated by RhoG, which can act both upstream of and in parallel with Rac1 and Cdc42 (Gauthier-Rouvière et al., 1998; Brugnera et al., 2002; Wennerberg et al., 2002; Katoh and Negishi, 2003; Samson et al., 2010). Further studies are needed to understand the molecular mechanisms that control these processes.

Contrary to our expectations, silencing SGEF does not affect apicobasal polarity when tested in 3D cysts. However, in the absence of SGEF, MDCK cysts display two distinct and severe phenotypes. First, instead of a single central lumen, most SGEF KD cysts display multiple lumens. These results agree with previous RNAi screens that identified SGEF as one of five human RhoGEFs with defects in lumen formation (Qin et al., 2010). The formation of cysts with multiple lumens may be caused by the loss of E-cadherin, as previous work has shown that E-cadherin KD cysts have multiple small lumens (Jia et al., 2011). ZO-1, which is also reduced in SGEF KD, may also contribute to the phenotype, as the average number of lumens increases in ZO-1–depleted cysts (Odenwald et al., 2017). Additionally, Dlg1 KD promotes multiple lumens, suggesting that the interaction between SGEF and Dlg1 may be important to specify a single lumen (Awad et al., 2013). Second, the formation of an open lumen is severely impaired in SGEF KD cysts, which form either very small or completely closed lumens. In MDCK cells grown in matrigel, the formation of an open lumen requires the polarized delivery of secretory vesicles that are targeted to the site of lumen initiation, where they fuse with the plasma membrane (Sigurbjörnsdóttir et al., 2014). The mechanism by which SGEF regulates the formation of an open lumen is not known, but previous work suggests it may be related to its newly revealed ability to bind Scribble, as Scribble function has been associated with lumen opening. When Scribble is silenced, cysts form with closed lumens in vitro (Yates et al., 2013; Hendrick et al., 2016), and in vivo, lungs from the Scribble mouse mutant Circletail are abnormally shaped with fewer airways that often lack a visible, open lumen (Yates et al., 2013). Again, as observed with the results in 2D monolayers, the scaffolding and catalytic activities of SGEF seem to independently regulate the two main cysts phenotypes observed; the scaffolding activity is sufficient to mediate lumen opening, whereas the catalytic activity is required for the regulation of lumen number.

Future experiments will focus on the molecular mechanisms that control the formation of the ternary complex and its role in the regulation of AJ and TJ function. It will also be interesting to characterize the spatiotemporal regulation of RhoG activity, identify RhoG's downstream effectors, and decipher the mechanisms by which they control E-cadherin stability and AJ function.

Materials and methods

Cell lines

HEK 293FT cells (Thermo Fisher Scientific) were used for all the overexpression and pulldown experiments unless indicated otherwise. MDCK II cells were a gift from I.G. Macara (Vanderbilt University, Nashville, TN). Caco-2 cells were a gift from W.S. Crawley (The University of Toledo, Toledo, OH). HEK 293FT and MDCK cells were grown in DMEM (GIBCO) containing 10% FBS and antibiotics (penicillin-streptomycin). Caco-2 cells were grown in DMEM supplemented with 10 mM L-glutamine containing 20% FBS and antibiotics (penicillin-streptomycin). All cell lines were grown at 37°C and 5% CO_2. All experiments were conducted with early passage cells that were passaged no more than 15 times. Mycoplasma was tested regularly by staining with Hoechst 33342 (AnaSpec Inc).

Antibodies

SGEF polyclonal antibodies were generated in rabbits using the following antigen located at SGEF's N terminus (DGESEVDFSSNSITPLWRRR; Pacific Immunologicals). The following antibodies were used in this study: RhoG (SC-26484, mouse monoclonal) 1:1,000 WB; Myc (9E10, SC-131, mouse monoclonal) 1:1,000 WB; Afadin (SC-74433, mouse monoclonal) 1:500 WB, 1:50 IF; Dlg1 (SC-9961, mouse monoclonal) 1:500 WB, 1:100 IF; Scribble (SC-11049, goat polyclonal) 1:250 WB, 1:25 IF; β-catenin (SC-7963, mouse monoclonal) 1:1,000 WB, 1:100 IF; p120-catenin (SC-13957, mouse monoclonal) 1:500 WB, 1:50 IF; and pan-cadherin (SC-515872, mouse monoclonal) 1:500 WB, 1:50 IF, all from Santa Cruz Biotechnology; E-cadherin (rr1, mouse monoclonal) 1:500 WB, 1:100 IF; and gp135 (3F2/D8, mouse monoclonal) 1:300 IF, from the Developmental Studies Hybridoma Bank at the University of Iowa; tubulin (T9028, mouse monoclonal) 1:10,000 WB, from Sigma-Aldrich; myosin IIB (D8H8, rabbit polyclonal) 1:500 WB, 1:50 IF, from Cell Signaling Technology; ZO-1 (339100, mouse monoclonal) 1:1,000 WB, 1:150 IF; GFP (MA5-15256, mouse monoclonal) 1:10,000 WB; 6x-His Tag (HIS.H8, mouse monoclonal) 1:3,000 WB; and cadherin-6 (2B6, rabbit polyclonal) 1:250 WB, 1:25 IF, from Thermo Fisher Scientific; myosin IIB (909901, rabbit polyclonal) 1:1,000 WB, 1:250 IF, from Biolegend; Alexa Fluor 488– and Alexa Fluor 594–conjugated anti-mouse-IgG and anti-rabbit-IgG secondary antibodies (A11008, A11001, A11005, A32733, and R37117), Alexa Fluor 594 (A-11032), and Alexa Fluor 647 (A22287) conjugated to phalloidin, from Thermo Fisher Scientific; HRP-conjugated anti-mouse-IgG, anti-rabbit-IgG, and anti-goat-IgG secondary antibodies from Jackson Immunoresearch (715-035-151, 711-035-152, and 705-035-147).

Plasmids and constructs

A list of plasmids used in the study is shown in Table S1.

Two-hybrid screening

A Matchmaker Gold Yeast Two-Hybrid System (Clontech) was used to screen for SGEF-interacting proteins. Full-length human SGEF was cloned into the "bait" vector pGBK7 and used to screen a mouse kidney pGADT7 cDNA library (>2.5 × 10^7 independent clones). Individual colonies containing potentially positive clones (126) were isolated and retested for interaction with SGEF, and false positives were discarded. The inserts from the positive clones were amplified by PCR and grouped according to their restriction pattern. Representative clones from each group were sequenced.

Lentiviral constructs and transduction

pLKO.1 Blast, Addgene 26655, was used to knock down SGEF in MDCK cells. pLKO.1 Blast lentiviral nontargeting shRNA CTRL was from Addgene 26701. The targeting shRNA sequence for canine SGEF is GGTGAAAAGAGGTGAGTTA (Qin et al., 2010). Lentiviruses were prepared by transfecting HEK293FT cells with pLKO.1 (6 µg), pMD2.G (0.8 µg), and pSPAX2 (4 µg) constructs (pMD2.G and pSPAX2 were a gift from Didier Trono, EPFL, Lausanne, Switzerland); Addgene plasmids 12259 and 12260). Cell culture medium was changed 24 h after transfection, and lentivirus was harvested 48 h after transfection. MDCK cells were infected with lentivirus particles overnight. The following day, the infection medium was removed and replaced with complete medium containing 10 µg/ml blasticidin to select for shRNA-expressing cells. Total cell lysates were subjected to WB analysis for protein expression as described above. For some shRNAs, single-cell colonies were isolated by serial dilution. pLenti-CMV-Hygro-Dest vector from Addgene 17454 was used to prepare stable MDCK cells expressing mNeon-SGEF constructs as described above. For overexpression and rescue experiments, MDCK cells were infected with lentivirus particles overnight and then selected with 600 ng/ml hygromycin.

Transfections and immunoprecipitation

HEK293FT cells were transfected using a standard calcium phosphate transfection method. Briefly, 50 µl of 2.5 M $CaCl_2$ was diluted to a final concentration of 0.25 M in MilliQ water. The DNA constructs to be transfected were added to the diluted $CaCl_2$ reagent and mixed by tapping gently. 500 µl of 2× HBS (Hepes Buffer Saline) (280 mM NaCl, 10 mM KCl, 1.5 mM Na_2HPO_4, 12 mM H_20, 50 mM Hepes, pH 7.05, and 12 mM glucose) was then added to the bottom of the tube, and the mixture was aerated gently by blowing bubbles with an empty 1-ml pipette at the bottom of the tube. The transfection mix was allowed to stand at room temperature for 30 s and then added dropwise to a 100-mm tissue culture dish of cells. Media were changed 24 h after transfection and cells harvested 48 h after transfection. The cells cultured on 100-mm tissue culture dishes were rinsed with PBS and then scraped into a lysis buffer containing 50 mM Tris-HCl, pH 7.4, 10 mM $MgCl_2$, 150 mM NaCl, 1% Triton X-100, and EZBlock protease inhibitor cocktail (BioVision). The supernatant was collected after centrifugation at 16,800 *g* for 10 min. For immunoblotting, lysates were boiled in 2× Laemmli buffer, and 20 µg of protein was resolved by SDS-PAGE. The proteins were transferred onto polyvinylidene fluoride and immunoblotted with the indicated antibodies. Immunocomplexes were visualized using the SuperSignal West Pico PLUS Chemiluminescent HRP substrate (Thermo Fisher Scientific). For immunoprecipitation, protein concentration was measured using DC protein assay reagent (BioRad) and equal amount of protein added to respective beads (ChromoTek GFP-Trap, myc-Trap, or mNeon-Trap

beads). Beads were incubated with lysates for 1 h at 4°C on a rotator, washed four times with lysis buffer, resuspended in 2× Laemmli buffer, and loaded on SDS polyacrylamide gels for WB analysis. For coimmunoprecipitation of the endogenous Scribble/SGEF/Dlg1 ternary complex, Caco-2 or MDCK cells grown in 100-mm tissue culture dishes were rinsed with PBS containing 10 mM EDTA and lysed using a modified lysis buffer (50 mM Tris-HCl, pH 7.4, 10 mM $MgCl_2$, 150 mM NaCl, 1% Triton X-100, 10 mM EDTA, and EZBlock protease inhibitor cocktail [BioVision]). The cell lysates were then incubated with anti-Dlg1 antibodies (or no antibodies: CTRL) at 4°C for 3 h. Protein G-Sepharose (GE) was then added and incubated overnight at 4°C. Immune complexes were recovered by centrifugation, washed three times with lysis buffer, and boiled in SDS sample buffer. Immune complexes were split into two aliquots (90% and 10%), which were run separately on SDS-PAGE gels and transferred to polyvinylidene fluoride membranes. The membranes with 90% of immune complexes were blotted for Scribble and SGEF, whereas those with 10% of immune complexes were blotted for Dlg1.

3D cyst culture

The day before cyst inoculation, MDCK cells were split into a 10-cm dish at a confluency of 1:10. On the day of plating, plates were washed two times followed by trypsinization using 0.25% trypsin, centrifuged at 1,200 rpm followed by two washes, and resuspended in calcium- and magnesium-free PBS. 2×10^3 cells were then plated on 100% matrigel on an eight-well glass-bottom µ-slide (Ibidi; 6 µl matrigel per well). Cells were then overlaid with 300 µl of 2% matrigel in DMEM. The cysts were grown for 4 d with a change of media on day 2. On day 4, cysts were fixed with 3.7% formaldehyde and processed for IF.

IF assays

The IF assays were performed as described earlier (García-Mata et al., 2003). Briefly, MDCK cells grown on coverslips or Transwell filters were fixed for 10 min with 3.7% paraformaldehyde and quenched with 10 mM ammonium chloride. Cells were then permeabilized with 0.1% Triton X-100 in PBS for 10 min. The coverslips were then washed with PBS and blocked in PBS, 2.5% goat serum (Sigma-Aldrich), and 0.2% Tween 20 for 5 min followed by 5-min blocking in PBS, 0.4% fish skin gelatin (Sigma-Aldrich), and 0.2% Tween 20. Cells were incubated with primary antibodies for 1 h at room temperature. The coverslips were then washed with PBS and 0.2% Tween 20 and incubated with Alexa Fluor 594 or 647 secondary antibodies for 45 min, washed as described above, and mounted on glass slides in ProLong Diamond Antifade Mountant (P36965; Thermo Fisher Scientific).

For 3D cysts, IF was performed as previously described (O'Brien et al., 2001). Briefly, samples were washed with PBS and fixed in 3.7% paraformaldehyde, washed, and then permeabilized with 0.2% Triton X-100 for 10 min. After blocking with 0.4% fish skin gelatin and 2.5% goat serum (30 min each), the cysts were incubated overnight at 4°C with primary antibodies in 2.5% goat serum. Primary antibodies were used at a concentration two times higher than that used for IF on coverslips. Cysts were then washed three times quickly, followed by 3 × 10-min washes with 0.2% Tween 20 in PBS. Secondary antibodies coupled with Alexa Fluor 488, 594, or 647 were incubated with the fixed specimens for 2–3 h at room temperature. Cysts were washed five times with 0.2% Tween in PBS and mounted in ProLong Diamond antifade reagent.

TEER measurements

The cells were plated onto 0.4-µm polyester membrane, 12-mm Transwell filters, at 5×10^5 cells per filter (Corning). Resistance measurements were performed 3 d later in triplicate using an EVOM Epithelial Voltohmmeter (World Precision Instruments). The values represent the average of three trials minus the background resistance. Values were normalized to those of CTRL cells (100%).

Confocal microscopy

Fluorescent confocal images were collected either using an inverted Olympus Fluoview 1000 microscope equipped with a 60× supercorrected PLAPON 60XOSC objective (NA = 1.4; working distance = 0.12 mm) and FV10-ASW software (*Xenopus* embryo studies) or using a Leica SP8 confocal microscope equipped with HyD detectors, a PlApo CS2 N 63×/1.4 oil objective, LAS X software (Leica), and a Hybrid superresolution package (HyVolution; MDCK studies).

Image processing and quantifications in MDCK cells

Deconvolution microscopy

To examine the localization of actin and myosin in MDCK cells, Z-section images were captured using the HyD detectors in the Leica SP8 confocal with the PlApo CS2 N 63×/1.4 objective, and the raw data were deconvolved using Huygens software (Scientific Volume Imaging) that accompanies the HyVolution package using standard settings.

Zigzag index measurements

The zigzag index was calculated as previously described (Tokuda et al., 2014). Briefly, BCJs were manually traced both freehand following exactly the lines of the junction, and with a straight line between the two TCJs encompassing the junction. The ratio of the freehand lines to that of straight lines was calculated and defined as the zigzag index. Around 100 cells were analyzed in a total of three independent experiments.

Quantification of junctional E-cadherin, β-catenin, p120-catenin, Scribble, and Dlg1

Line scans (6-µm line drawn perpendicular to the center of junctions) were performed using ImageJ as follows. Brightest point projections of z-stacked images were created using ImageJ. At least two fields from two independent experiments were used for quantification (≥200 junctions). The intensity profiles were manually centered around the highest peak for each condition.

Quantification of height of MDCK cells

Confocal images were captured in XZ mode using a Leica SP8 confocal microscope. Leica LAS X software was used for

measurement of height at the tallest point of a cell. At least 50 cells from 10 individual images in at least three different experiments were used to calculate height.

Quantification of ZO-1 intensities at junctions of MDCK cells

Brightest point projections of z-stacked images were created using ImageJ. A rectangle of size 4 × 1.5-µm length was aligned with its longer side parallel to the length of a junction. Average intensities were plotted using Prism 8 (GraphPad).

Quantification of Afadin TCJ/BCJ intensity ratio

Brightest point projections of z-stacked images were created using ImageJ. A circle of 2.5 µm diameter was placed at the center of a TCJ and its corresponding BCJ. Average Afadin intensities (TCJ/BCJ) were plotted using Prism 8 (GraphPad).

Xenopus embryos and microinjections

All studies conducted using *Xenopus* embryos strictly adhered to the compliance standards of the US Department of Health and Human Services Guide for the Care and Use of Laboratory Animals and were approved by the University of Michigan's Institutional Animal Care and Use Committee. *Xenopus* embryos were collected, in vitro fertilized, dejellied, and microinjected with mRNAs for fluorescent probes using methods described previously (Reyes et al., 2014). Briefly, embryos were injected in the animal hemisphere at the two-cell stage (each cell injected twice) for fixed phalloidin staining experiments, and either at the two-cell stage (each cell injected twice) or at the four-cell stage (each cell injected once) for live imaging experiments and allowed to develop to gastrula stage (stages 10.5–12; Nieuwkoop and Faber, 1994). The constructs used for these experiments and their sources are summarized in Table S1. The conditions used for microinjection are listed in Table S2.

F-actin staining in *Xenopus*

Gastrula-stage embryos were fixed and stained using methods described previously (Reyes et al., 2014) with the following changes: embryos were fixed with 1.5% formaldehyde, 0.25% glutaraldehyde, 0.2% Triton X-100, and 0.88× MT fix buffer (1× MT buffer: 80 mM K-Pipes, 5 mM EGTA, and 1 mM $MgCl_2$, pH 6.8) and blocked in Tris-buffered saline (50 mM Tris and 150 mM NaCl, pH 7.4) containing 10% FBS, 5% DMSO, and 0.1% NP-40 overnight at room temperature. F-actin was stained with phalloidin Alexa Fluor 568 (Life Technologies), 1:100. Phalloidin was added during the initial fixation step to help preserve delicate medial-apical actin structures.

Image processing and quantification in *Xenopus*

All images were processed and analyzed with ImageJ. En face views shown in figures are brightest point Z-projections. Side views shown are averaged projections or single Z-planes (see figure legends). Videos were converted to avi files using ImageJ (JPEG compressed, 15 frames/s). Graphs and statistical analysis were done using GraphPad Prism 5.

Quantification of SGEF and RhoG localization relative to AJs and TJs in live embryos

The apico-basal intensity profiles of mNeon-tagged SGEF and RhoG were quantified as described in Higashi et al. (2018). Briefly, z-stack images of 30–40 optical slices with 0.5 µm thickness were taken from multiple embryos (see numbers in figure legend). Each junction was quantified as follows: a 50 × 50-pixel (px)-square region of interest of a straight section of the junction was cropped from the original image and reoriented, yielding a stack of 50 X-Z side views of the junction. This side view stack was flattened using an average intensity projection. Because the junction is often not straight from apical to basal, the intensities at each z position were flattened into 1 px using a brightest point projection. Fluorescence intensity profiles were determined for TagBFP-ZO-1 (TJ marker), PLEKHA7-mCherry (AJ marker), and either mNeon-SGEF or mNeon-RhoG for each junction. The intensity profiles from multiple junctions were then normalized and averaged to produce the graphs shown in Fig. 4.

Quantification of junctional mNeon-SGEF WT, mNeon-SGEF 1–227, and mNeon-SGEF 228–871 in live embryos

Brightest point projections of z-stack images were generated using ImageJ. From each image, 14 to 20 BCJ junctions were traced with a 1-px-wide segmented line, and mean intensities were measured. Cytosolic intensities were measured by shifting each segmented line into the cytosolic region 5–10 px to the side of the junction. Ratios of junctional to cytosolic SGEF were calculated.

Quantification of junctional F-actin in fixed phalloidin-stained embryos

Line scans were performed using ImageJ as follows. Brightest point projections of z-stacked images were created using ImageJ. Junctions were traced with a 5-px-wide segmented line. Average intensities and junction lengths were measured. All junctions fully visible in each image were included. The data were graphed using Prism.

Quantification of medial-apical F-actin in fixed phalloidin-stained embryos

Brightest point projections of z-stacked images were created using ImageJ. The entire medial-apical surface of each cell was outlined, and average intensities were measured. All cells fully visible in each image were measured. The intensity data were graphed using Prism.

Quantification of junctional vinculin intensity in live embryos

Line scans were performed using ImageJ as follows. Brightest point projections of z-stacked images were created using ImageJ. Junctions were traced with a 1-px-wide segmented line, and average intensities were measured. Five to seven junctions were measured from each image. Since mRNA expression levels vary from embryo to embryo and even within each embryo membrane probe intensities were used to normalize vinculin intensity data. These data were graphed using Prism (GraphPad).

Statistical analysis

Each experiment was performed at least three times unless indicated. Each dataset was tested for normality using the D'Agostino test in Prism8 (GraphPad). Statistical significance was then determined using either a *t* test (two-tailed, unpaired), with data that passed the normality test, or a Mann–Whitney *U* test, as indicated in the figure legends, using Prism8 (GraphPad).

Protein expression and purification

Polymerase chain reaction was used to amplify the human Scribble PDZ1 domain (residues 725–815) from the full-length DNA sequence. The amplified DNA was ligated into a modified pET21α vector (Novagen) that contained an N-terminal 6XHis affinity tag and a tobacco etch virus (rTEV) protease cleavage site. The nucleotide coding sequence of the pET21α-PDZ1 vector was verified by automated DNA sequencing (University of Iowa, DNA Facility). Protein expression was conducted in BL21(DE3) (Invitrogen) *Escherichia coli* cells. Typically, *E. coli* cells were grown at 37°C in Luria-Bertani medium supplemented with ampicillin (100 µg/ml) under vigorous agitation until an A600 of 0.6–0.8 was reached. Cultures were subsequently cooled to 18°C, and protein expression was induced by the addition of isopropyl 1-thio-β-d-galactopyranoside to 1 mM final concentration. Induced cells were incubated for an additional 16–18 h at 18°C and harvested by centrifugation.

The Scribble PDZ1 domain was purified by nickel-chelate (GE Healthcare) and size-exclusion chromatography (GE Healthcare). The N-terminal 6XHis affinity tag was removed by proteolysis with recombinant rTEV protease for 36 h at 4°C. Undigested protein, cleaved 6XHis tag, and His-tagged rTEV were separated from Scribble PDZ domains by nickel-chelate chromatography. The digested proteins were further purified with S75 size-exclusion chromatography with the desired final buffer. The final yield was ∼50 mg of PDZ protein (>98% pure as judged by SDS-PAGE) from 1 liter of culture. Samples were used immediately or lyophilized and stored at −80°C.

Synthetic SGEF peptide

The SGEF iPBM (residues 42–55: ac-KPNGLLITDFPVED$_{CONH2}$) peptide was chemically synthesized by GenScript and judged to be >95% pure by analytical HPLC and mass spectrometry. The SGEF iPBM peptide was acetylated at the N terminus and amidated at the C terminus. The peptide concentration was determined by absorbance measurements (A280) using the predicted extinction coefficient from the amino acid sequence.

Crystallization and data collection

Crystallization conditions for the free and peptide-bound forms of the Scribble PDZ1 domain were determined by the hanging-drop, vapor-diffusion method using high-throughput screens automated by a Mosquito drop setter (TTP LabTech). Equal volumes (200 nl) of precipitant and protein (10–23 mg/ml; 20 mM Tris base and 50 mM NaCl, pH 7.5) alone or with 5–10 molar equivalents of peptide were used for crystal screens. Crystals of the free Scribble PDZ1 domain were obtained in condition 40 of the index screen (0.1 M citric acid, pH 3.5, and 25% [wt/vol] PEG 3350; Hampton Research), while the Scribble PDZ1/SGEF-PDZ$_{peptide}$ complex formed crystals in condition 29 of the index screen (60% [vol/vol] Tacsimate, pH 7.0; Hampton Research).

Initial crystal diffraction screening was achieved with a CuK rotating anode beam; full x-ray diffraction datasets for structure determination were collected using a RDI CMOS_8M detector at 0.5 steps over 180° for the free crystal and over 120° for the peptide-bound form at beamline 4.2.2 at the Advanced Light Source. The free Scribble PDZ1 domain crystallized in space group $C222_1$ with one molecule per asymmetric unit. The SGEF-PDZ$_{peptide\text{-}bound}$ complex crystallized in space group $P4_32_12$ with one molecule in the asymmetric unit. Proper space group handedness was verified by analysis of the electron density.

Structure determination and structure refinement

The XDS program (Kabsch, 2010a,b) was used for indexing, integration, and scaling of the diffraction data. The program PHASER (McCoy et al., 2007) was used for the initial phasing of both the free Scribble PDZ1 structure and the Scribble PDZ1/SGEF-PDZ$_{peptide}$ complex structure using the previously determined Scribble PDZ1 structure (PDB ID: 2W4F) as the template. Automated model building was performed using ARP/wARP (Langer et al., 2008). The early stages of refinement used Refmac (Murshudov et al., 1997), while the later stages used the PHENIX software suite (Adams et al., 2010). Final polishing and refinement were carried in PDB_REDO (Joosten et al., 2014). Electron density visualization and manual model building were done in Coot (Emsley et al., 2010). R_{free} values were calculated using 10% of the reflections selected randomly and not used in the refinement (Brünger, 1992). The structures were refined to 1.6 Å in the free form and to 1.1 Å in the complex form. The refinement statistics are shown in Table S3. Structural alignment and figures were prepared with PyMOL (Schrodinger, Version 1.8).

Online supplemental material

Fig. S1 shows mapping the binding domains of SGEF, Scribble, and Dlg1 interaction. Fig. S2 shows that SGEF and RhoG localize to junctions in MDCK cells. Fig. S3 shows that SGEF regulates the establishment of junction in MDCK cells. Fig. S4 shows that SGEF signals through the ROCK/myosin pathway to induce contractility in MDCK cells. Fig. S5 shows that he catalytic activity of SGEF is required for lumen formation in MDCK cysts grown in matrigel. Table S1 shows constructs used in this study. Table S2 shows *Xenopus* microinjection parameters. Table S3 shows crystallographic data and refinement statistics. Video 1 shows CTRL *Xenopus* embryos imaged using a confocal microscope. Video 2 shows SGEF OE *Xenopus* embryos imaged using a confocal microscope.

Acknowledgments

We would like to thank I. Macara (Vanderbilt University, Nashville, TN), A. Fanning (University of North Carolina at Chapel Hill, Chapel Hill, NC), C.M. Van Itallie (National Institutes of Health, Bethesda, MD), K. Mostov (University of California, San Francisco, San Francisco, CA), and S.W. Crawley

(University of Toledo, Toledo, OH) for reagents and advice. We thank W.M. Bement (University of Wisconsin-Madison, Madison, WI) for pCS2+/Lifeact-mRFP and E.M. Munro (The University of Chicago, Chicago, IL) for the myosin intrabody, SF9. We would like to acknowledge use of resources at the Carver College of Medicine's Protein and Crystallography Facility at the University of Iowa. We would like to acknowledge Dr. Lokesh Gakhar (University of Iowa, Iowa City, IA) and Jay Nix (beamline 4.2.2, Advanced Light Source, Berkeley, CA) for help collecting diffraction datasets. In addition, this research used resources of the Advanced Light Source, which is a US Department of Energy Office of Science User Facility under contract no. DE-AC02-05CH11231.

This work was supported by National Institutes of Health grants 1R15CA199101, 1R21CA194776, and 1R03CA197227 to R. Garcia-Mata and R01 GM112794 to A.L. Miller; a National Science Foundation Graduate Research Fellowship and Rackham Merit Fellowship to T.R. Arnold; American Heart Association grant 15GRNT25740021 to E.J. Fuentes; and Associazione Italiana per la Ricerca sul Cancro grant 18578 to L. Banks.

The authors declare no competing financial interests.

Author contributions: Conceptualization: S. Awadia, E.J. Fuentes, A.L. Miller, and R. Garcia-Mata; investigation: S. Awadia, F. Huq, T.R. Arnold, S. Goicoechea, Y.J. Sun, T. Hou, G. Kreider-Letterman, and R. Garcia-Mata; visualization: S. Awadia, F. Huq, T.R. Arnold, S. Goicoechea, Y.J. Sun, T. Hou, G. Kreider-Letterman, E.J. Fuentes, A.L. Miller, and R. Garcia-Mata; formal analysis: S. Awadia, F. Huq, T.R. Arnold, S. Goicoechea, Y.J. Sun, and T. Hou; resources: P. Massimi and L. Banks; writing: S. Awadia, S. Goicoechea, E.J. Fuentes, A.L. Miller, and R. Garcia-Mata; funding acquisition: E.J. Fuentes, A.L. Miller, and R. Garcia-Mata; and supervision: R. Garcia-Mata. All authors read and approved the final manuscript.

Submitted: 20 November 2018
Revised: 18 March 2019
Accepted: 12 April 2019

References

Adams, P.D., P.V. Afonine, G. Bunkóczi, V.B. Chen, I.W. Davis, N. Echols, J.J. Headd, L.-W. Hung, G.J. Kapral, R.W. Grosse-Kunstleve, et al. 2010. PHENIX: a comprehensive Python-based system for macromolecular structure solution. *Acta Crystallogr. D Biol. Crystallogr.* 66:213–221. https://doi.org/10.1107/S0907444909052925

Aijaz, S., F. D'Atri, S. Citi, M.S. Balda, and K. Matter. 2005. Binding of GEF-H1 to the tight junction-associated adaptor cingulin results in inhibition of Rho signaling and G1/S phase transition. *Dev. Cell.* 8:777–786. https://doi.org/10.1016/j.devcel.2005.03.003

Anderson, J.M., and C.M. Van Itallie. 2009. Physiology and function of the tight junction. *Cold Spring Harb. Perspect. Biol.* 1:a002584. https://doi.org/10.1101/cshperspect.a002584

Audebert, S., C. Navarro, C. Nourry, S. Chasserot-Golaz, P. Lécine, Y. Bellaiche, J.L. Dupont, R.T. Premont, C. Sempéré, J.M. Strub, et al. 2004. Mammalian Scribble forms a tight complex with the betaPIX exchange factor. *Curr. Biol.* 14:987–995. https://doi.org/10.1016/j.cub.2004.05.051

Awad, A., S. Sar, R. Barré, C. Cariven, M. Marin, J.P. Salles, C. Erneux, D. Samuel, and A. Gassama-Diagne. 2013. SHIP2 regulates epithelial cell polarity through its lipid product, which binds to Dlg1, a pathway subverted by hepatitis C virus core protein. *Mol. Biol. Cell.* 24:2171–2185. https://doi.org/10.1091/mbc.e12-08-0626

Bilder, D., and N. Perrimon. 2000. Localization of apical epithelial determinants by the basolateral PDZ protein Scribble. *Nature.* 403:676–680. https://doi.org/10.1038/35001108

Bilder, D., M. Schober, and N. Perrimon. 2003. Integrated activity of PDZ protein complexes regulates epithelial polarity. *Nat. Cell Biol.* 5:53–58. https://doi.org/10.1038/ncb897

Blum, M., E.M. De Robertis, J.B. Wallingford, and C. Niehrs. 2015. Morpholinos: Antisense and Sensibility. *Dev. Cell.* 35:145–149. https://doi.org/10.1016/j.devcel.2015.09.017

Bonello, T.T., and M. Peifer. 2018. Scribble: A master scaffold in polarity, adhesion, synaptogenesis, and proliferation. *J. Cell Biol.* 218:742–756.

Brenman, J.E., and D.S. Bredt. 1997. Synaptic signaling by nitric oxide. *Curr. Opin. Neurobiol.* 7:374–378. https://doi.org/10.1016/S0959-4388(97)80065-7

Breznau, E.B., A.C. Semack, T. Higashi, and A.L. Miller. 2015. MgcRacGAP restricts active RhoA at the cytokinetic furrow and both RhoA and Rac1 at cell-cell junctions in epithelial cells. *Mol. Biol. Cell.* 26:2439–2455. https://doi.org/10.1091/mbc.E14-11-1553

Brugnera, E., L. Haney, C. Grimsley, M. Lu, S.F. Walk, A.C. Tosello-Trampont, I.G. Macara, H. Madhani, G.R. Fink, and K.S. Ravichandran. 2002. Unconventional Rac-GEF activity is mediated through the Dock180-ELMO complex. *Nat. Cell Biol.* 4:574–582. https://doi.org/10.1038/ncb824

Brünger, A.T. 1992. Free R value: a novel statistical quantity for assessing the accuracy of crystal structures. *Nature.* 355:472–475. https://doi.org/10.1038/355472a0

Buckley, C.D., J. Tan, K.L. Anderson, D. Hanein, N. Volkmann, W.I. Weis, W.J. Nelson, and A.R. Dunn. 2014. Cell adhesion. The minimal cadherin-catenin complex binds to actin filaments under force. *Science.* 346:1254211. https://doi.org/10.1126/science.1254211

Capaldo, C.T., and I.G. Macara. 2007. Depletion of E-cadherin disrupts establishment but not maintenance of cell junctions in Madin-Darby canine kidney epithelial cells. *Mol. Biol. Cell.* 18:189–200. https://doi.org/10.1091/mbc.e06-05-0471

Caria, S., C.M. Magtoto, T. Samiei, M. Portela, K.Y.B. Lim, J.Y. How, B.Z. Stewart, P.O. Humbert, H.E. Richardson, and M. Kvansakul. 2018. *Drosophila melanogaster* Guk-holder interacts with the Scribbled PDZ1 domain and regulates epithelial development with Scribbled and Discs Large. *J. Biol. Chem.* 293:4519–4531. https://doi.org/10.1074/jbc.M117.817528

Cereijido, M., E.S. Robbins, W.J. Dolan, C.A. Rotunno, and D.D. Sabatini. 1978. Polarized monolayers formed by epithelial cells on a permeable and translucent support. *J. Cell Biol.* 77:853–880. https://doi.org/10.1083/jcb.77.3.853

Chen, A., H. Beetham, M.A. Black, R. Priya, B.J. Telford, J. Guest, G.A. Wiggins, T.D. Godwin, A.S. Yap, and P.J. Guilford. 2014. E-cadherin loss alters cytoskeletal organization and adhesion in non-malignant breast cells but is insufficient to induce an epithelial-mesenchymal transition. *BMC Cancer.* 14:552. https://doi.org/10.1186/1471-2407-14-552

Choi, W., B.R. Acharya, G. Peyret, M.A. Fardin, R.M. Mège, B. Ladoux, A.S. Yap, A.S. Fanning, and M. Peifer. 2016. Remodeling the zonula adherens in response to tension and the role of afadin in this response. *J. Cell Biol.* 213:243–260. https://doi.org/10.1083/jcb.201506115

Dow, L.E., A.M. Brumby, R. Muratore, M.L. Coombe, K.A. Sedelies, J.A. Trapani, S.M. Russell, H.E. Richardson, and P.O. Humbert. 2003. hScrib is a functional homologue of the Drosophila tumour suppressor Scribble. *Oncogene.* 22:9225–9230. https://doi.org/10.1038/sj.onc.1207154

Ellerbroek, S.M., K. Wennerberg, W.T. Arthur, J.M. Dunty, D.R. Bowman, K.A. DeMali, C. Der, and K. Burridge. 2004. SGEF, a RhoG guanine nucleotide exchange factor that stimulates macropinocytosis. *Mol. Biol. Cell.* 15:3309–3319. https://doi.org/10.1091/mbc.e04-02-0146

Elsum, I., L. Yates, P.O. Humbert, and H.E. Richardson. 2012. The Scribble-Dlg-Lgl polarity module in development and cancer: from flies to man. *Essays Biochem.* 53:141–168. https://doi.org/10.1042/bse0530141

Emsley, P., B. Lohkamp, W.G. Scott, and K. Cowtan. 2010. Features and development of Coot. *Acta Crystallogr. D Biol. Crystallogr.* 66:486–501. https://doi.org/10.1107/S0907444910007493

Fanning, A.S., C.M. Van Itallie, and J.M. Anderson. 2012. Zonula occludens-1 and -2 regulate apical cell structure and the zonula adherens cytoskeleton in polarized epithelia. *Mol. Biol. Cell.* 23:577–590. https://doi.org/10.1091/mbc.e11-09-0791

Farquhar, M.G., and G.E. Palade. 1963. Junctional complexes in various epithelia. *J. Cell Biol.* 17:375–412. https://doi.org/10.1083/jcb.17.2.375

García-Mata, R., and K. Burridge. 2007. Catching a GEF by its tail. *Trends Cell Biol.* 17:36–43. https://doi.org/10.1016/j.tcb.2006.11.004

García-Mata, R., T. Szul, C. Alvarez, and E. Sztul. 2003. ADP-ribosylation factor/COPI-dependent events at the endoplasmic reticulum-Golgi interface are regulated by the guanine nucleotide exchange factor GBF1. *Mol. Biol. Cell.* 14:2250–2261. https://doi.org/10.1091/mbc.e02-11-0730

García-Mata, R., A.D. Dubash, L. Sharek, H.S. Carr, J.A. Frost, and K. Burridge. 2007. The nuclear RhoA exchange factor Net1 interacts with proteins of the Dlg family, affects their localization, and influences their tumor suppressor activity. *Mol. Cell. Biol.* 27:8683–8697. https://doi.org/10.1128/MCB.00157-07

Gateff, E., and H.A. Schneiderman. 1974. Developmental capacities of benign and malignant neoplasms ofDrosophila. *Wilhelm Roux Arch. Entwickl. Mech. Org.* 176:23–65. https://doi.org/10.1007/BF00577830

Gauthier-Rouvière, C., E. Vignal, M. Mériane, P. Roux, P. Montcourier, and P. Fort. 1998. RhoG GTPase controls a pathway that independently activates Rac1 and Cdc42Hs. *Mol. Biol. Cell.* 9:1379–1394. https://doi.org/10.1091/mbc.9.6.1379

Goicoechea, S.M., A. Zinn, S.S. Awadia, K. Snyder, and R. Garcia-Mata. 2017. A RhoG-mediated signaling pathway that modulates invadopodia dynamics in breast cancer cells. *J. Cell Sci.* 130:1064–1077.

Gumbiner, B., and K. Simons. 1986. A functional assay for proteins involved in establishing an epithelial occluding barrier: identification of a uvomorulin-like polypeptide. *J. Cell Biol.* 102:457–468. https://doi.org/10.1083/jcb.102.2.457

Gumbiner, B., B. Stevenson, and A. Grimaldi. 1988. The role of the cell adhesion molecule uvomorulin in the formation and maintenance of the epithelial junctional complex. *J. Cell Biol.* 107:1575–1587. https://doi.org/10.1083/jcb.107.4.1575

Hara, Y., M. Shagirov, and Y. Toyama. 2016. Cell Boundary Elongation by Non-autonomous Contractility in Cell Oscillation. *Curr. Biol.* 26:2388–2396. https://doi.org/10.1016/j.cub.2016.07.003

Hendrick, J., M. Franz-Wachtel, Y. Moeller, S. Schmid, B. Macek, and M.A. Olayioye. 2016. The polarity protein Scribble positions DLC3 at adherens junctions to regulate Rho signaling. *J. Cell Sci.* 129:3583–3596. https://doi.org/10.1242/jcs.190074

Higashi, T., T.R. Arnold, R.E. Stephenson, K.M. Dinshaw, and A.L. Miller. 2016. Maintenance of the Epithelial Barrier and Remodeling of Cell-Cell Junctions during Cytokinesis. *Curr. Biol.* 26:1829–1842. https://doi.org/10.1016/j.cub.2016.05.036

Higashi, T., R.E. Stephenson, and A.L. Miller. 2018. Comprehensive analysis of formin localization in Xenopus epithelial cells. *Mol. Biol. Cell.* 30:82–95.

Hildebrand, J.D. 2005. Shroom regulates epithelial cell shape via the apical positioning of an actomyosin network. *J. Cell Sci.* 118:5191–5203. https://doi.org/10.1242/jcs.02626

Hillier, B.J., K.S. Christopherson, K.E. Prehoda, D.S. Bredt, and W.A. Lim. 1999. Unexpected modes of PDZ domain scaffolding revealed by structure of nNOS-syntrophin complex. *Science.* 284:812–815. https://doi.org/10.1126/science.284.5415.812

Holeiter, G., A. Bischoff, A.C. Braun, B. Huck, P. Erlmann, S. Schmid, R. Herr, T. Brummer, and M.A. Olayioye. 2012. The RhoGAP protein Deleted in Liver Cancer 3 (DLC3) is essential for adherens junctions integrity. *Oncogenesis.* 1:e13. https://doi.org/10.1038/oncsis.2012.13

Iden, S., and J.G. Collard. 2008. Crosstalk between small GTPases and polarity proteins in cell polarization. *Nat. Rev. Mol. Cell Biol.* 9:846–859. https://doi.org/10.1038/nrm2521

Ivanov, A.I., C. Young, K. Den Beste, C.T. Capaldo, P.O. Humbert, P. Brennwald, C.A. Parkos, and A. Nusrat. 2010. Tumor suppressor scribble regulates assembly of tight junctions in the intestinal epithelium. *Am. J. Pathol.* 176:134–145. https://doi.org/10.2353/ajpath.2010.090220

Jackson, B.C., I.A. Ivanova, and L. Dagnino. 2015. An ELMO2-RhoG-ILK network modulates microtubule dynamics. *Mol. Biol. Cell.* 26:2712–2725. https://doi.org/10.1091/mbc.E14-10-1444

Jia, L., F. Liu, S.H. Hansen, M.B. Ter Beest, and M.M. Zegers. 2011. Distinct roles of cadherin-6 and E-cadherin in tubulogenesis and lumen formation. *Mol. Biol. Cell.* 22:2031–2041. https://doi.org/10.1091/mbc.e11-01-0038

Joosten, R.P., F. Long, G.N. Murshudov, and A. Perrakis. 2014. The PDB_REDO server for macromolecular structure model optimization. *IUCrJ.* 1:213–220. https://doi.org/10.1107/S2052252514009324

Kabsch, W. 2010a. Integration, scaling, space-group assignment and post-refinement. *Acta Crystallogr. D Biol. Crystallogr.* 66:133–144. https://doi.org/10.1107/S0907444909047374

Kabsch, W. 2010b. XDS. *Acta Crystallogr. D Biol. Crystallogr.* 66:125–132. https://doi.org/10.1107/S0907444909047337

Kalluri, R., and R.A. Weinberg. 2009. The basics of epithelial-mesenchymal transition. *J. Clin. Invest.* 119:1420–1428. https://doi.org/10.1172/JCI39104

Katoh, H., and M. Negishi. 2003. RhoG activates Rac1 by direct interaction with the Dock180-binding protein Elmo. *Nature.* 424:461–464. https://doi.org/10.1038/nature01817

Katoh, M., and M. Katoh. 2004. Identification and characterization of human GUKH2 gene in silico. *Int. J. Oncol.* 24:1033–1038.

Katoh, H., H. Yasui, Y. Yamaguchi, J. Aoki, H. Fujita, K. Mori, and M. Negishi. 2000. Small GTPase RhoG is a key regulator for neurite outgrowth in PC12 cells. *Mol. Cell. Biol.* 20:7378–7387. https://doi.org/10.1128/MCB.20.19.7378-7387.2000

Katoh, H., K. Hiramoto, and M. Negishi. 2006. Activation of Rac1 by RhoG regulates cell migration. *J. Cell Sci.* 119:56–65. https://doi.org/10.1242/jcs.02720

Krishna Subbaiah, V., P. Massimi, S.S. Boon, M.P. Myers, L. Sharek, R. Garcia-Mata, and L. Banks. 2012. The invasive capacity of HPV transformed cells requires the hDlg-dependent enhancement of SGEF/RhoG activity. *PLoS Pathog.* 8:e1002543. https://doi.org/10.1371/journal.ppat.1002543

Langer, G., S.X. Cohen, V.S. Lamzin, and A. Perrakis. 2008. Automated macromolecular model building for X-ray crystallography using ARP/wARP version 7. *Nat. Protoc.* 3:1171–1179. https://doi.org/10.1038/nprot.2008.91

Laprise, P., A. Viel, and N. Rivard. 2004. Human homolog of disc-large is required for adherens junction assembly and differentiation of human intestinal epithelial cells. *J. Biol. Chem.* 279:10157–10166. https://doi.org/10.1074/jbc.M309843200

Legouis, R., F. Jaulin-Bastard, S. Schott, C. Navarro, J.P. Borg, and M. Labouesse. 2003. Basolateral targeting by leucine-rich repeat domains in epithelial cells. *EMBO Rep.* 4:1096–1102. https://doi.org/10.1038/sj.embor.7400006

Lim, K.Y.B., N.J. Gödde, P.O. Humbert, and M. Kvansakul. 2017. Structural basis for the differential interaction of Scribble PDZ domains with the guanine nucleotide exchange factor βtruc. *J. Biol. Chem.* 292:20425–20436.

Liu, X., T.R. Shepherd, A.M. Murray, Z. Xu, and E.J. Fuentes. 2013. The structure of the Tiam1 PDZ domain/phospho-syndecan1 complex reveals a ligand conformation that modulates protein dynamics. *Structure.* 21:342–354. https://doi.org/10.1016/j.str.2013.01.004

Lohia, M., Y. Qin, and I.G. Macara. 2012. The Scribble polarity protein stabilizes E-cadherin/p120-catenin binding and blocks retrieval of E-cadherin to the Golgi. *PLoS One.* 7:e51130. https://doi.org/10.1371/journal.pone.0051130

London, T.B., H.J. Lee, Y. Shao, and J. Zheng. 2004. Interaction between the internal motif KTXXXI of Idax and mDvl PDZ domain. *Biochem. Biophys. Res. Commun.* 322:326–332. https://doi.org/10.1016/j.bbrc.2004.07.113

Mack, N.A., and M. Georgiou. 2014. The interdependence of the Rho GTPases and apicobasal cell polarity. *Small GTPases.* 5:10. https://doi.org/10.4161/21541248.2014.973768

Mathew, D., L.S. Gramates, M. Packard, U. Thomas, D. Bilder, N. Perrimon, M. Gorczyca, and V. Budnik. 2002. Recruitment of scribble to the synaptic scaffolding complex requires GUK-holder, a novel DLG binding protein. *Curr. Biol.* 12:531–539. https://doi.org/10.1016/S0960-9822(02)00758-3

McCoy, A.J., R.W. Grosse-Kunstleve, P.D. Adams, M.D. Winn, L.C. Storoni, and R.J. Read. 2007. Phaser crystallographic software. *J. Appl. Cryst.* 40:658–674. https://doi.org/10.1107/S0021889807021206

Mechler, B.M., W. McGinnis, and W.J. Gehring. 1985. Molecular cloning of lethal(2)giant larvae, a recessive oncogene of Drosophila melanogaster. *EMBO J.* 4:1551–1557. https://doi.org/10.1002/j.1460-2075.1985.tb03816.x

Métais, J.Y., C. Navarro, M.J. Santoni, S. Audebert, and J.P. Borg. 2005. hScrib interacts with ZO-2 at the cell-cell junctions of epithelial cells. *FEBS Lett.* 579:3725–3730. https://doi.org/10.1016/j.febslet.2005.05.062

Mu, Y., P. Cai, S. Hu, S. Ma, and Y. Gao. 2014. Characterization of diverse internal binding specificities of PDZ domains by yeast two-hybrid screening of a special peptide library. *PLoS One.* 9:e88286. https://doi.org/10.1371/journal.pone.0088286

Munjal, A., and T. Lecuit. 2014. Actomyosin networks and tissue morphogenesis. *Development.* 141:1789–1793. https://doi.org/10.1242/dev.091645

Murshudov, G.N., A.A. Vagin, and E.J. Dodson. 1997. Refinement of macromolecular structures by the maximum-likelihood method. *Acta Crystallogr. D Biol. Crystallogr.* 53:240–255. https://doi.org/10.1107/S0907444996012255

Navarro, C., S. Nola, S. Audebert, M.J. Santoni, J.P. Arsanto, C. Ginestier, S. Marchetto, J. Jacquemier, D. Isnardon, A. Le Bivic, et al. 2005. Junctional recruitment of mammalian Scribble relies on E-cadherin engagement. *Oncogene.* 24:4330–4339. https://doi.org/10.1038/sj.onc.1208632

Ngok, S.P., and P.Z. Anastasiadis. 2013. Rho GEFs in endothelial junctions: Effector selectivity and signaling integration determine junctional response. *Tissue Barriers.* 1:e27132. https://doi.org/10.4161/tisb.27132

Ngok, S.P., W.H. Lin, and P.Z. Anastasiadis. 2014. Establishment of epithelial polarity--GEF who's minding the GAP? *J. Cell Sci.* 127:3205–3215. https://doi.org/10.1242/jcs.153197

Nieuwkoop, P.D., and J. Faber. 1994. *Normal Table of Xenopus Laevis (Daudin).* Garland Science, New York, NY.

Nishimura, T., H. Honda, and M. Takeichi. 2012. Planar cell polarity links axes of spatial dynamics in neural-tube closure. *Cell.* 149:1084–1097. https://doi.org/10.1016/j.cell.2012.04.021

O'Brien, L.E., T.S. Jou, A.L. Pollack, Q. Zhang, S.H. Hansen, P. Yurchenco, and K.E. Mostov. 2001. Rac1 orientates epithelial apical polarity through effects on basolateral laminin assembly. *Nat. Cell Biol.* 3:831–838. https://doi.org/10.1038/ncb0901-831

O'Brien, L.E., M.M. Zegers, and K.E. Mostov. 2002. Opinion: Building epithelial architecture: insights from three-dimensional culture models. *Nat. Rev. Mol. Cell Biol.* 3:531–537. https://doi.org/10.1038/nrm859

Odenwald, M.A., W. Choi, A. Buckley, N. Shashikanth, N.E. Joseph, Y. Wang, M.H. Warren, M.M. Buschmann, R. Pavlyuk, J. Hildebrand, et al. 2017. ZO-1 interactions with F-actin and occludin direct epithelial polarization and single lumen specification in 3D culture. *J. Cell Sci.* 130:243–259. https://doi.org/10.1242/jcs.188185

Ojakian, G.K., and R. Schwimmer. 1988. The polarized distribution of an apical cell surface glycoprotein is maintained by interactions with the cytoskeleton of Madin-Darby canine kidney cells. *J. Cell Biol.* 107:2377–2387. https://doi.org/10.1083/jcb.107.6.2377

Patel, J.C., and J.E. Galán. 2006. Differential activation and function of Rho GTPases during Salmonella-host cell interactions. *J. Cell Biol.* 175:453–463. https://doi.org/10.1083/jcb.200605144

Penkert, R.R., H.M. DiVittorio, and K.E. Prehoda. 2004. Internal recognition through PDZ domain plasticity in the Par-6-Pals1 complex. *Nat. Struct. Mol. Biol.* 11:1122–1127. https://doi.org/10.1038/nsmb839

Petit, M.M., S.M. Meulemans, P. Alen, T.A. Ayoubi, E. Jansen, and W.J. Van de Ven. 2005. The tumor suppressor Scrib interacts with the zyxin-related protein LPP, which shuttles between cell adhesion sites and the nucleus. *BMC Cell Biol.* 6:1. https://doi.org/10.1186/1471-2121-6-1

Qin, Y., C. Capaldo, B.M. Gumbiner, and I.G. Macara. 2005. The mammalian Scribble polarity protein regulates epithelial cell adhesion and migration through E-cadherin. *J. Cell Biol.* 171:1061–1071. https://doi.org/10.1083/jcb.200506094

Qin, Y., W.H. Meisen, Y. Hao, and I.G. Macara. 2010. Tuba, a Cdc42 GEF, is required for polarized spindle orientation during epithelial cyst formation. *J. Cell Biol.* 189:661–669. https://doi.org/10.1083/jcb.201002097

Raman, A.S., K.I. White, and R. Ranganathan. 2016. Origins of Allostery and Evolvability in Proteins: A Case Study. *Cell.* 166:468–480. https://doi.org/10.1016/j.cell.2016.05.047

Ratheesh, A., G.A. Gomez, R. Priya, S. Verma, E.M. Kovacs, K. Jiang, N.H. Brown, A. Akhmanova, S.J. Stehbens, and A.S. Yap. 2012. Centralspindlin and α-catenin regulate Rho signalling at the epithelial zonula adherens. *Nat. Cell Biol.* 14:818–828. https://doi.org/10.1038/ncb2532

Ratheesh, A., R. Priya, and A.S. Yap. 2013. Coordinating Rho and Rac: the regulation of Rho GTPase signaling and cadherin junctions. *Prog. Mol. Biol. Transl. Sci.* 116:49–68. https://doi.org/10.1016/B978-0-12-394311-8.00003-0

Ren, J., L. Feng, Y. Bai, H. Pei, Z. Yuan, and W. Feng. 2015. Interdomain interface-mediated target recognition by the Scribble PDZ34 supramodule. *Biochem. J.* 468:133–144. https://doi.org/10.1042/BJ20141473

Reyes, C.C., M. Jin, E.B. Breznau, R. Espino, R. Delgado-Gonzalo, A.B. Goryachev, and A.L. Miller. 2014. Anillin regulates cell-cell junction integrity by organizing junctional accumulation of Rho-GTP and actomyosin. *Curr. Biol.* 24:1263–1270. https://doi.org/10.1016/j.cub.2014.04.021

Rodriguez-Boulan, E., and I.G. Macara. 2014. Organization and execution of the epithelial polarity programme. *Nat. Rev. Mol. Cell Biol.* 15:225–242. https://doi.org/10.1038/nrm3775

Röper, K. 2013. Supracellular actomyosin assemblies during development. *Bioarchitecture.* 3:45–49. https://doi.org/10.4161/bioa.25339

Rossman, K.L., C.J. Der, and J. Sondek. 2005. GEF means go: turning on RHO GTPases with guanine nucleotide-exchange factors. *Nat. Rev. Mol. Cell Biol.* 6:167–180. https://doi.org/10.1038/nrm1587

Samson, T., C. Welch, E. Monaghan-Benson, K.M. Hahn, and K. Burridge. 2010. Endogenous RhoG is rapidly activated after epidermal growth factor stimulation through multiple guanine-nucleotide exchange factors. *Mol. Biol. Cell.* 21:1629–1642. https://doi.org/10.1091/mbc.e09-09-0809

Sharma, S., S.L. Ang, M. Shaw, D.A. Mackey, J. Gécz, J.W. McAvoy, and J.E. Craig. 2006. Nance-Horan syndrome protein, NHS, associates with epithelial cell junctions. *Hum. Mol. Genet.* 15:1972–1983. https://doi.org/10.1093/hmg/ddl120

Shen, L., C.R. Weber, D.R. Raleigh, D. Yu, and J.R. Turner. 2011. Tight junction pore and leak pathways: a dynamic duo. *Annu. Rev. Physiol.* 73:283–309. https://doi.org/10.1146/annurev-physiol-012110-142150

Sigurbjörnsdóttir, S., R. Mathew, and M. Leptin. 2014. Molecular mechanisms of de novo lumen formation. *Nat. Rev. Mol. Cell Biol.* 15:665–676. https://doi.org/10.1038/nrm3871

Songyang, Z., A.S. Fanning, C. Fu, J. Xu, S.M. Marfatia, A.H. Chishti, A. Crompton, A.C. Chan, J.M. Anderson, and L.C. Cantley. 1997. Recognition of unique carboxyl-terminal motifs by distinct PDZ domains. *Science.* 275:73–77. https://doi.org/10.1126/science.275.5296.73

Sousa, S., D. Cabanes, C. Archambaud, F. Colland, E. Lemichez, M. Popoff, S. Boisson-Dupuis, E. Gouin, M. Lecuit, P. Legrain, and P. Cossart. 2005. ARHGAP10 is necessary for alpha-catenin recruitment at adherens junctions and for Listeria invasion. *Nat. Cell Biol.* 7:954–960. https://doi.org/10.1038/ncb1308

Stephenson, R.E., and A.L. Miller. 2017. Tools for live imaging of active Rho GTPases in Xenopus. *Genesis.* 55:e22998.

Stevenson, B.R., J.M. Anderson, D.A. Goodenough, and M.S. Mooseker. 1988. Tight junction structure and ZO-1 content are identical in two strains of Madin-Darby canine kidney cells which differ in transepithelial resistance. *J. Cell Biol.* 107:2401–2408. https://doi.org/10.1083/jcb.107.6.2401

Stewart, D.B., A.I. Barth, and W.J. Nelson. 2000. Differential regulation of endogenous cadherin expression in Madin-Darby canine kidney cells by cell-cell adhesion and activation of beta-catenin signaling. *J. Biol. Chem.* 275:20707–20716. https://doi.org/10.1074/jbc.M000467200

Takai, Y., and H. Nakanishi. 2003. Nectin and afadin: novel organizers of intercellular junctions. *J. Cell Sci.* 116:17–27. https://doi.org/10.1242/jcs.00167

Tang, V. 2017. Cell-cell adhesion interface: rise of the lateral membrane. *F1000 Res.* 6:276. https://doi.org/10.12688/f1000research.10680.1

Tcherkezian, J., and N. Lamarche-Vane. 2007. Current knowledge of the large RhoGAP family of proteins. *Biol. Cell.* 99:67–86. https://doi.org/10.1042/BC20060086

Terry, S.J., C. Zihni, A. Elbediwy, E. Vitiello, I.V. Leefa Chong San, M.S. Balda, and K. Matter. 2011. Spatially restricted activation of RhoA signalling at epithelial junctions by p114RhoGEF drives junction formation and morphogenesis. *Nat. Cell Biol.* 13:159–166. https://doi.org/10.1038/ncb2156

Tinkle, C.L., T. Lechler, H.A. Pasolli, and E. Fuchs. 2004. Conditional targeting of E-cadherin in skin: insights into hyperproliferative and degenerative responses. *Proc. Natl. Acad. Sci. USA.* 101:552–557. https://doi.org/10.1073/pnas.0307437100

Tokuda, S., T. Higashi, and M. Furuse. 2014. ZO-1 knockout by TALEN-mediated gene targeting in MDCK cells: involvement of ZO-1 in the regulation of cytoskeleton and cell shape. *PLoS One.* 9:e104994. https://doi.org/10.1371/journal.pone.0104994

Toret, C.P., C. Collins, and W.J. Nelson. 2014. An Elmo-Dock complex locally controls Rho GTPases and actin remodeling during cadherin-mediated adhesion. *J. Cell Biol.* 207:577–587. https://doi.org/10.1083/jcb.201406135

Tripathi, V., N.C. Popescu, and D.B. Zimonjic. 2012. DLC1 interaction with α-catenin stabilizes adherens junctions and enhances DLC1 antioncogenic activity. *Mol. Cell. Biol.* 32:2145–2159. https://doi.org/10.1128/MCB.06580-11

Tunggal, J.A., I. Helfrich, A. Schmitz, H. Schwarz, D. Günzel, M. Fromm, R. Kemler, T. Krieg, and C.M. Niessen. 2005. E-cadherin is essential for in vivo epidermal barrier function by regulating tight junctions. *EMBO J.* 24:1146–1156. https://doi.org/10.1038/sj.emboj.7600605

Umeda, K., J. Ikenouchi, S. Katahira-Tayama, K. Furuse, H. Sasaki, M. Nakayama, T. Matsui, S. Tsukita, M. Furuse, and S. Tsukita. 2006. ZO-1 and ZO-2 independently determine where claudins are polymerized in tight-junction strand formation. *Cell.* 126:741–754. https://doi.org/10.1016/j.cell.2006.06.043

Valdivia, A., S.M. Goicoechea, S. Awadia, A. Zinn, and R. Garcia-Mata. 2017. Regulation of circular dorsal ruffles, macropinocytosis, and cell

migration by RhoG and its exchange factor, Trio. *Mol. Biol. Cell.* 28: 1768–1781. https://doi.org/10.1091/mbc.e16-06-0412

van Buul, J.D., M.J. Allingham, T. Samson, J. Meller, E. Boulter, R. García-Mata, and K. Burridge. 2007. RhoG regulates endothelial apical cup assembly downstream from ICAM1 engagement and is involved in leukocyte trans-endothelial migration. *J. Cell Biol.* 178:1279–1293. https://doi.org/10.1083/jcb.200612053

Van Itallie, C.M., A.S. Fanning, A. Bridges, and J.M. Anderson. 2009. ZO-1 - stabilizes the tight junction solute barrier through coupling to the perijunctional cytoskeleton. *Mol. Biol. Cell.* 20:3930–3940. https://doi.org/10.1091/mbc.e09-04-0320

Walsh, G.S., P.K. Grant, J.A. Morgan, and C.B. Moens. 2011. Planar polarity pathway and Nance-Horan syndrome-like 1b have essential cell-autonomous functions in neuronal migration. *Development.* 138: 3033–3042. https://doi.org/10.1242/dev.063842

Watabe, M., A. Nagafuchi, S. Tsukita, and M. Takeichi. 1994. Induction of polarized cell-cell association and retardation of growth by activation of the E-cadherin-catenin adhesion system in a dispersed carcinoma line. *J. Cell Biol.* 127:247–256. https://doi.org/10.1083/jcb.127.1.247

Wennerberg, K., S.M. Ellerbroek, R.Y. Liu, A.E. Karnoub, K. Burridge, and C.J. Der. 2002. RhoG signals in parallel with Rac1 and Cdc42. *J. Biol. Chem.* 277:47810–47817. https://doi.org/10.1074/jbc.M203816200

Wong, H.C., A. Bourdelas, A. Krauss, H.J. Lee, Y. Shao, D. Wu, M. Mlodzik, D.L. Shi, and J. Zheng. 2003. Direct binding of the PDZ domain of Dishevelled to a conserved internal sequence in the C-terminal region of Frizzled. *Mol. Cell.* 12:1251–1260. https://doi.org/10.1016/S1097-2765(03)00427-1

Woods, D.F., and P.J. Bryant. 1991. The discs-large tumor suppressor gene of Drosophila encodes a guanylate kinase homolog localized at septate junctions. *Cell.* 66:451–464. https://doi.org/10.1016/0092-8674(81)90009-X

Woolner, S., A.L. Miller, and W.M. Bement. 2009. Imaging the cytoskeleton in live Xenopus laevis embryos. *Methods Mol. Biol.* 586:23–39. https://doi.org/10.1007/978-1-60761-376-3_2

Yates, L.L., C. Schnatwinkel, L. Hazelwood, L. Chessum, A. Paudyal, H. Hilton, M.R. Romero, J. Wilde, D. Bogani, J. Sanderson, et al. 2013. Scribble is required for normal epithelial cell-cell contacts and lumen morphogenesis in the mammalian lung. *Dev. Biol.* 373:267–280. https://doi.org/10.1016/j.ydbio.2012.11.012

Yonemura, S., Y. Wada, T. Watanabe, A. Nagafuchi, and M. Shibata. 2010. alpha-Catenin as a tension transducer that induces adherens junction development. *Nat. Cell Biol.* 12:533–542. https://doi.org/10.1038/ncb2055

Zebda, N., Y. Tian, X. Tian, G. Gawlak, K. Higginbotham, A.B. Reynolds, A.A. Birukova, and K.G. Birukov. 2013. Interaction of p190RhoGAP with C-terminal domain of p120-catenin modulates endothelial cytoskeleton and permeability. *J. Biol. Chem.* 288:18290–18299. https://doi.org/10.1074/jbc.M112.432757